This is a Just Accepted version, keep updated with https://doi.org/10.26599/EMD.2026.9370102
Energy Materials and Devices **2026, 4(3), 9370102**

Graphical Abstract

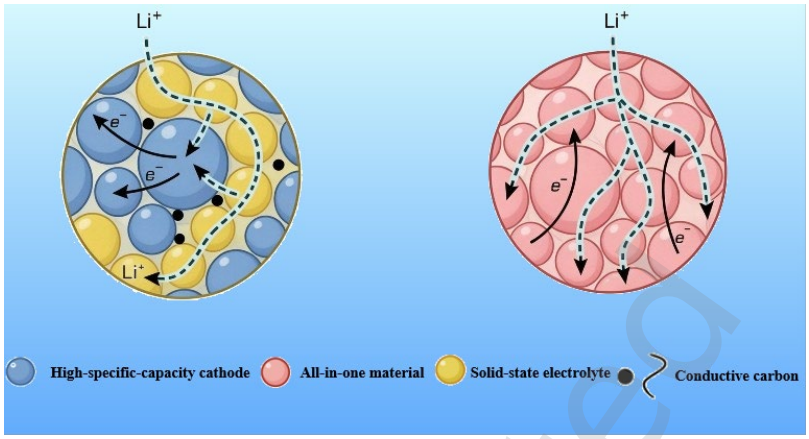

Fe-based halides serve as both solid electrolytes and high-capacity cathodes in all-solid-state lithium batteries, offering a low-cost, dual-function pathway toward simplified architecture and high energy density.

This is a Just Accepted version, keep updated with https://doi.org/10.26599/EMD.2026.9370102
Energy Materials and Devices **2026, 4(3), 9370102**

Article Type: Review Article

Materials engineering of Fe-based halides for low-cost and high-energy-density all-solid-state lithium batteries: A review and perspective

Chonggui Lei,[1,2] Zuxin Long,[1,2] Lang Yuan,[3] Liansheng Li,[2]* Geng Li,[2,4]* Yu Lu,[4] and Qinghua Liang[1,2]*

[1]*School of Metallurgical Engineering, Jiangxi University of Science and Technology, Ganzhou 341000, China*

[2]*Key Laboratory of Rare Earths, Ganjiang Innovation Academy, Chinese Academy of Sciences, Ganzhou 341119, China*

[3]*School of Chemistry and Chemical Engineering, Jiangxi University of Science and Technology, Ganzhou 341000, China*

[4]*China Rare Earth Group Research Institute, Shenzhen, Guangdong 518000, China*

* Address correspondence to Liansheng Li, lsli@gia.cas.cn; Geng Li, geng_li@regcc.cn; Qinghua Liang, qhliang@gia.cas.cn

Received: May 7, 2026 / **Revised:** June 19, 2026 / **Accepted:** June 22, 2026

ABSTRACT: All-solid-state lithium batteries (ASSLBs) are considered a promising next-generation energy storage technology due to their enhanced safety and potential for high energy density. However, their practical deployment is constrained by challenges such as immature manufacturing processes and the high cost of key materials. Fe-based halides (FBHs) have recently emerged as compelling material candidates to address these issues, benefiting from their low cost, structural tunability, and inherent multifunctionality. This review highlights the unique dual-function of FBHs in ASSLBs, wherein they can serve simultaneously or separately as solid-state electrolytes with decent ionic conductivity and as high-capacity cathodes featuring reversible redox chemistry. We begin by discussing the structural characteristics and

cost advantages of FBHs. Subsequently, we examine their applications as solid electrolytes and as cathodes in full-cell configurations, with an emphasis on interfacial compatibility and electrochemical performance. Finally, we outline the remaining challenges and perspectives on the practical implementation of FBHs in ASSLBs. This review is expected to provide a systematic understanding of the dual-function potential of FBHs and to offer significant guidance for the development of low-cost and high-energy-density ASSLBs.

KEYWORDS

extra capacity, halide, redox-active catholyte, solid-state battery, solid-state electrolyte

This is a Just Accepted version, keep updated with https://doi.org/10.26599/EMD.2026.9370102
Energy Materials and Devices **2026, 4(3), 9370102**

1 Introduction

The field of energy storage technology is currently undergoing a profound transformation. With growing range anxiety in electric vehicles and the increasing integration of renewable energy into power grids, the demand for large-scale, high-safety energy storage systems has intensified. Consequently, developing next-generation energy storage technologies that overcome the limitations of conventional lithium-ion batteries (LIBs) has become a global priority. Although LIBs dominate the market, they rely on flammable liquid organic electrolytes and are approaching their theoretical energy density limits, while posing significant safety risks due to thermal runaway[1]. All-solid-state lithium batteries (ASSLBs), which replace liquid electrolytes with non-flammable solid-state electrolytes (SSEs), are widely regarded as a promising solution to simultaneously address the challenges of safety and energy density. They have therefore attracted substantial investment from both the research community and industry[2-4].

The core advantages of ASSLBs originate from their all-solid-state configuration. First, they eliminate risks associated with electrolyte leakage, volatilization, and decomposition, thereby offering intrinsic safety[5]. Second, certain SSEs, particularly sulfides and halides, exhibit exceptionally high lithium-ion conductivity at room temperature (RT)[6-8]. Their wide electrochemical windows enable pairing with high-energy-density cathodes, such as lithium-rich manganese-based materials, as well as lithium metal anodes. Moreover, ASSLBs offer a broader operating temperature range and the potential for extended calendar life[9].

Despite these advantages, transitioning ASSLBs from laboratory to industrial application presents formidable challenges involving materials and interfaces. At the material level, an ideal SSE is expected to simultaneously possess high RT ionic conductivity (>1 mS cm^{-1}), a wide electrochemical window, good stability against electrodes, ease of processing, and low cost. However, all currently developed systems have their respective shortcomings. For example, oxide electrolytes, such as the doped $Li_7La_3Zr_2O_{12}$, exhibit high chemical stability but suffer from high interfacial impedance.

Sulfide-based SSEs (e.g., Li_6PS_5Cl) offer extremely high conductivity but are air-sensitive and prone to reactions with high-voltage cathodes[10,11]. Polymer-based SSEs provide good processability but are limited by low RT conductivity and a narrow voltage window[12]. At the interface level, the physical instability of solid-solid contacts between electrodes and the SSEs, compounded by contact failure owing to volume changes during charge-discharge cycles, results in substantially increased interfacial impedance[13,14]. Simultaneously, chemical and electrochemical instability between the electrolyte and lithium metal anodes can trigger continuous interfacial degradation and accelerate dendrite growth[15-17]. These interconnected challenges underscore the urgent need for new SSEs that combine excellent overall performance with superior interfacial compatibility.

In 2018, Asano et al. prepared trigonal-phase Li_3YCl_6[18] and monoclinic-phase Li_3YBr_6, which exhibited room-temperature ionic conductivities of 0.51 and 1.7 $mS{\cdot}cm^{-1}$, respect-tively. Notably, Li_3YCl_6 demonstrated favorable chemical and electrochemical compatibility with uncoated $LiCoO_2$ (LCO) cathodes. Thermodynamic calculations revealed that SSEs possess high oxidative stabilities, rendering them suitable to be compatible with high-voltage cathode materials[19]. Typically, the oxidation potentials of Li_3YCl_6 and Li_3YBr_6 were determined to be 4.21 and 3.15 V, respectively[20]. The F-type SSEs exhibit an even wider electro-chemical stability window, with oxidation and reduction potentials of 6.36 and 0.36 V, respectively [19]. Since then, SSEs have garnered widespread attention in the ASSLB field. Various high-performance SSEs have been thus developed, with Li_3MX_6 compounds as prototypical examples. SSEs display diverse crystal structures, including trigonal-phase Li_2ZrCl_6[21] and Li_3ErCl_6[22] and Li_3HoCl_6[23], orthorhombic-phase Li_3YBr_6[24] and Li_3HoBr_6[25,26], and monoclinic-phase Li_3ScCl_6[27] and $LiTaCl_6$[28] and $Li_{3-x}Y_{1-x}Hf_xCl_6$[29]. More innovatively, the role of halide extends beyond SSEs[30]. Certain transition metal halides, such as FeF_3 and $FeCl_3$, can serve as high-capacity conversion-type cathodes, leveraging multi-electron transfer to deliver specific capacities exceeding 300 mAh g^{-1}, far beyond those of conventional intercalation-type cathodes[31-33]. This dual-function

capability, acting as both an ion-conducting medium and an energy storage host, enables an integrated design strategy within a single material family, providing a novel platform for constructing ASSLBs with higher energy density and simplified interfaces. Despite these promising prospects, early development of halide-based SSEs relied heavily on scarce or expensive metallic elements like indium, making high raw material costs a major barrier to large-scale commercialization[34-37].

The emergence of Fe-based halides (FBHs) shows great promise to solve the above backdrop. Iron is the fourth most abundant element on Earth, offering extremely low cost and environmental friendliness. Initially, researchers attempted to partially or fully replace precious metals with iron to develop low-cost halide SSEs. However, subsequent studies revealed that FBHs are far more than mere cheap substitutes. Through judicious crystal and electronic structure design, they achieve more advantages in terms of cost, performance, and functionality. As SSEs, doping strategies with high-valent cations, such as Fe^{3+} in materials like $Li_{2+x}Hf_{1-x}Fe_xCl_6$[38], can optimize lithium-ion migration pathways while introducing additional charge carriers, achieving an ionic conductivity exceeding 0.9 mS cm^{-1}, comparable to that of precious metal-based pristine SSEs. As cathodes, materials such as $FeCl_3$ exhibit a flat discharge plateau as high as 3.8 V (vs Li^+/Li) and ultra-long cycling stability over more than 1000 cycles, while compounds like $Li_xFe_{1.2}Cl_4$ pioneer an integrated cathode paradigm that inherently possesses both ionic and electronic conductivity, eliminating the need for additional SSEs or conductive additives[58]. In terms of functional integration, FBHs blur the traditional boundaries between cathodes and SSEs, enabling the construction of active composites that combine energy storage and ion-transport functions. This fundamentally simplifies battery architecture and holds great promise for enhancing volumetric energy density. Thus, FBHs represent a paradigm shift from a substitution mindset to an innovation mindset. They are not merely a solution to cost challenges but also a key to unlocking new battery chemistries and novel device architectures.

In this review, we systematically summarize recent advances in FBHs for ASSLBs and provide a forward-looking perspective on their future development. We first outline

the fundamental physicochemical properties, crystal structure families, and cost advantages of FBHs. We then highlight doping modification strategies for their use as high-performance SSEs, focusing on ion transport mechanisms and interfacial compatibility with high-voltage cathodes. Subsequently, we shift focus to the breakthroughs of FBHs as high-performance cathodes, with a detailed discussion of their coupled intercalation-conversion mechanisms, high-voltage conversion reactions, and the emerging integrated cathode design. Finally, we discuss the key challenges currently facing the field, such as air stability and compatibility with lithium metal, and offer perspectives on future research directions.

2 Fundamental Properties and Structural Chemistry of Fe-Based Halides

Among the diverse material families explored for ASSLBs, FBHs are increasingly attracted by their rich crystal structures and exceptional compositional tunability. Their most compelling feature, however, lies not in the performance of any single compound but in the inherent flexibility of their crystal architectures, which function as a versatile "chemical LEGO" platform. By rationally controlling cation types and ratios or through anion substitution, a continuous structural landscape can be obtained, ranging from two-dimensional layered networks to three-dimensional frameworks, and from highly ordered configurations to long-range disordered states. This structural versatility serves as the fundamental basis for the designability and optimization of their electrochemical properties, enabling tailored functionalities that are central to their dual-role capability in ASSLBs[53].

2.1 Crystal Structure Families and Structural Characteristics

FBHs exhibit a remarkable diversity of crystal structures, ranging from layered motifs to three-dimensional frameworks, and from highly ordered arrangements to long-range disordered configurations. This structural richness provides the foundation for tailoring their electrochemical properties. As shown in **Figure 1a**, classic $FeCl_3$ adopts a typical O1-type layered structure[39]. Its structural complexity arises from the honeycomb-like ordering of Fe^{3+}/vacancies within the layers and the intergrowth of two stacking modes

along the c-axis ($\bar{R}3$ and $\bar{P}31m$)[40,41]. This stacking disorder reveals the intricacy of ion migration pathways in layered materials and provides a basis for subsequent structural tuning to optimize transport channels. Based on this, researchers have intentionally induced the collapse of the layered architecture through anion doping, such as fluorine substitution in FeOCl, yielding an amorphous phase characterized by long-range disorder yet locally featuring low-energy-barrier channels (**Figure 1b**). This demonstrates that controlled disruption of layered structures can instead create an environment conducive to rapid ion diffusion[49-52].

Through various strategies such as heterovalent cation doping, site occupation regulation, and valence state mixing, it is possible to achieve multi-level design of phase stability, ion distribution, and transport network. As shown in **Figures 1c-d**, the structural landscape ranges from the ordered distribution in $LiFeCl_4$, where Fe^{3+} occupies tetrahedral sites, and Li^+ occupies octahedral sites, to the formation of a pure *C2/m* phase in $Li_{2.9}Fe_{0.9}Zr_{0.1}Cl_6$[42,43]. The introduction of heterovalent cations not only stabilizes specific phases but also redistributes ions within the structure by favoring particular coordination environments[44,48]. In Li_2FeCl_4 and Li_6FeCl_8, controlled concentrations of lithium vacancies are intentionally introduced by partially occupying Li sites with Fe^{2+} (**Figures 1e-f**). These vacancies are not merely defects but rather designed highways that provide essential sites for Li^+ hopping. As in $Li_{1.3}Fe_{1.2}Cl_4$, where Fe and Li mix at specific Wyckoff sites, a stable and interconnected three-dimensional mixed-conduction framework was constructed[53-57].

Recently, the non-stoichiometric FBH of the $Li_{1.3}Fe_{1.2}Cl_4$ compound was prepared by mixing Fe^{2+} and Fe^{3+} (**Figure 1g**). Its orthorhombic *Cmmm* structure is not a simple derivative of any known phase but rather a novel, stable three-dimensional framework formed by edge-sharing of distinct coordination polyhedra[58]. This structural innovation, achieved by controlling the valence state of the transition metal and overall charge balance, significantly expands the compositional space and structural diversity of FBHs.

Overall, FBHs exhibit a rich configurational landscape, from the layered disorder of

$FeCl_3$ to the ordered three-dimensional framework of $Li_{1.3}Fe_{1.2}Cl_4$, profoundly demonstrating the high structural tunability. This property intricately links synthetic chemistry, structural analysis, and electrochemical performance. Leveraging this tunability to establish precise composition-structure-property relationships would enable the rational design and preparation of FBHs with targeted architectures, tailored to meet the specific voltage, capacity, and rate capability requirements of ASSLBs.

2.2 Elemental Abundance and Cost Advantages

FBHs derive a formidable cost advantage from their elemental composition. As one of the most abundant transition metals in Earth's crust (~4.7 wt%), iron benefits from high production volumes and historically stable, low prices. The halogen components further reinforce this advantage. Chlorine is primarily sourced from ubiquitous NaCl deposits, while bromine is widely distributed in brines, both serving as fundamental, low-cost chemical feedstocks. This stands in stark contrast to the critical, supply-constrained metals that underpin current commercial cathodes, such as cobalt, which is geographically concentrated and price-volatile, and nickel, which is subject to demand-driven price surges.

Beyond low-cost, FBHs exhibit compelling electrochemical performance, with $FeCl_3$ exemplifying this dual promise[32]. Its market price is only about 1–2% that of conventional cathodes, highlighting a substantial affordability advantage (**Figure 1h**). Remarkably, $FeCl_3$ demonstrates electrochemical performance comparable to or even surpassing that of commercial cathodes such as lithium iron phosphate (LFP) (**Figure 1i**). It delivers a higher operating voltage (3.65 V vs. 3.4 V), competitive capacity (165 mAh g^{-1} vs. 170 mAh g^{-1}), and higher gravimetric energy density (602 Wh kg^{-1} vs. 578 Wh kg^{-1}). As shown in **Figure 1j**, the cost of $FeCl_3$ was calculated to be USD 0.86 kWh^{-1}, which is lower than the cost of current cathodes, which ranged from USD 39 kWh^{-1} to USD 125 kWh^{-1}. Additionally, its low Young's modulus enhances flexibility for dense composite electrodes. Although $FeCl_3$ exhibits a lower theoretical density, its estimated volumetric energy density exceeds 1500 Wh L^{-1}, rivalling that of lithium nickel manganese cobalt oxide.

By leveraging earth-abundant elements, FBHs achieve ultra-low material costs while matching or exceeding the electrochemical metrics of incumbent cathode materials. Their favorable packing density and mechanical flexibility further benefit electrode processing. This unique combination of resource sustainability, cost-effectiveness, and high performance positions FBHs as a highly promising candidate for next-generation ASSLBs with high-energy-density.

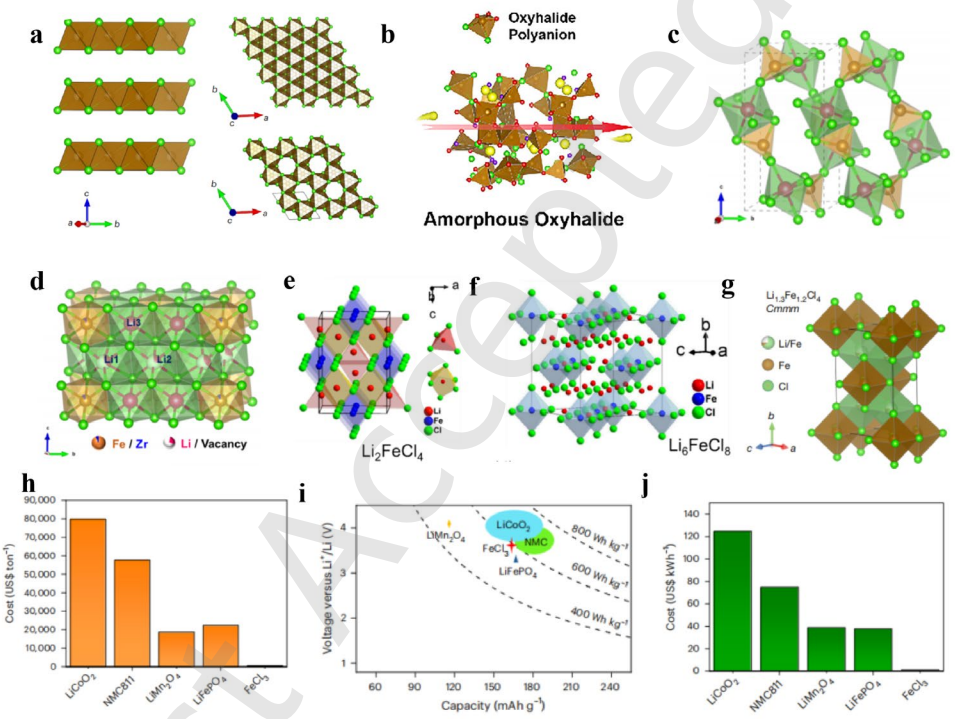

Figure 1. Structural diagrams of different FBHs. (a) Side view of the layered structure and the anion stacking of pristine $FeCl_3$. Reproduced with permission from Ref.[32] ©2024, Nature. (b) Amorphous LFFOC-*x* CAMs. Reproduced with permission from Ref.[49] ©2025, Wiley. (c, d) Crystal structures of $LiFeCl_4$ (*P21/c*) and $Li_{2.9}Fe_{0.9}Zr_{0.1}Cl_6$ (*C2/m*) projected along the a-axis, respectively (where Fe, Zr, Li, and Cl are represented by brown, blue, pink, and green spheres, respectively). Reproduced with permission from Ref.[43] ©2024, American Chemical Society. (e) The crystal structure of Li_2FeCl_4 with Li-Cl tetrahedrons (red) and octahedrons (yellow). Reproduced with permission from Ref.[53] ©2024, American Chemical Society. (f) The crystal structures of Li_6FeCl_8. Reproduced with permission from Ref. [53] ©2024, American Chemical Society. (g) Crystal structure of $Li_{1.3}Fe_{1.2}Cl_4$ with a *Cmmm* space group. Reproduced with permission from Ref.[58] ©2024, Nature. The cost chart

and electrochemical performance of $FeCl_3$. (h) market prices of different cathode materials and (i) Voltage and specific capacity of different cathode materials, and (j) calculated cost of cathode materials per kilowatt hour. Reproduced with permission from Ref.[32] ©2025, Nature.

3 Fe-Based Halides as Solid-State Electrolytes

The SSE serves as the heart of ASSLBs, directly governing the ion transport efficiency, operating voltage window, and cycle life. Research on FBHs as solid electrolytes has undergone a notable evolution, transitioning from the initial concept of low-cost substitution to a distinct research thrust centered on achieving performance breakthroughs through precise crystal structure engineering.

3.1 Ion Transport Mechanisms

When FBHs are used as SSEs, ionic conductivity is a key indicator for evaluating their practical application potential. Current research suggests that the main factors affecting lithium-ion transport include crystal structure, lithium vacancy concentration, and structural dimensionality. The following sections will discuss the impact of these factors on lithium-ion transport in the FBH-based solid-state electrolytes.

Crystal structure plays a crucial role in lithium-ion transport in FBHs. For instance, the Li_3FeCl_6 typically contains about 13.7% of a low-ionic-conductivity $P2_1/c$ impurity phase. The doping of Zr^{4+} effectively suppresses the formation of this impurity phase. As demonstrated in $Li_{2.9}Fe_{0.9}Zr_{0.1}Cl_6$[43], the impurity phase content is reduced to 2.4%, and the ionic conductivity consequently increases by an order of magnitude. When the Zr doping level is further raised to 30%, a pure *C2/m* phase can be obtained. Previous studies have shown that FBHs adopting the *C2/m* structure possess a three-dimensional lithium-ion diffusion network, which serves as the structural basis for their high ionic conductivity. The amorphous FBHs also generally show improved ion transport. For example, subjecting the F^--doped FeOCl to a halogen-exchange reaction can transform the material from a crystalline layered structure into an amorphous state and create a fast lithium-ion conduction pathway[49]. As such, the ionic conductivity improves from an extremely low level (10^{-8} S cm^{-1}) to a high value of 10^{-4} S cm^{-1}. Amorphous

1.2LiOH-$FeCl_3$ prepared from LiOH and $FeCl_3$ also delivers an ionic conductivity as high as 6.1 mS cm^{-1} [70]. The mechanism study reveals that Li^+ transport in such amorphous FBH is not simply hopping between fixed crystal structure sites; instead, it is intimately coupled with the cooperative motion of the flexible network. Namely, the Li^+ migration and structural rearrangement of the network are coupled together.

Besides, the ion transport in FBHs is highly affected by the lithium vacancy concentration. For example, researchers employed an Fe^{2+} self-doping strategy to achieve precise control over the lithium vacancy concentration in Li_2FeCl_4[59] and Li_6FeCl_8. Each Fe^{2+} ion replaces two Li^+ ions, directly introducing one lithium vacancy into the lattice and thereby effectively increasing the carrier concentration. Meanwhile, owing to the difference in ionic radii between Fe^{2+} and Li^+, this doping also induces a slight lattice expansion and widens the migration bottleneck[49]. More importantly, this aliovalent substitution introduces pronounced local disorder into the lithium sublattice. The cation arrangement no longer retains strict long-range order, and the local coordination environments and electrostatic potential distributions become distorted. This leads to a flattening of the potential energy landscape, thereby further lowering the ion-hopping energy barrier. This synergistic interplay by increasing vacancy concentration, enlarging channel dimensions, and local structural disorder enhances the room-temperature ionic conductivity of $Li_{1.8}Fe_{1.1}Cl_4$ by more than two orders of magnitude relative to its parent material.

Structural dimensionality also plays a critical role in the ion transport performance of FBHs. Low-dimensional (one- or two-dimensional) channels are highly susceptible to interruption by grain boundaries, antisite defects, or local blockages, whereas three-dimensionally interconnected diffusion networks can provide abundant detour pathways, ensuring reliable long-range conduction. For example, the ion transport in the spinel-derived phase c-Li_2FeCl_4 further corroborates this point. This phase retains an intact three-dimensional lithium-ion percolation network with every diffusion pathway remaining fully connected[62]. Through compositional tuning, the orthorhombic phase o-$Li_{1.75}FeCl_4$ likewise constructs highly efficient three-

dimensional conduction channels, achieving an ionic conductivity as high as 0.39 mS cm^{-1}, thereby demonstrating the superiority of three-dimensional diffusion pathways over low-dimensional structures. Meanwhile, the non-stoichiometric compound $Li_{1.3}Fe_{1.2}Cl_4$ delivers an impressive ionic conductivity of 2.28×10^{-4} S cm^{-1} due to the three-dimensional structural integrity enabled by the complex composition[58]. These results suggest that the ionic conductivity of FBHs can achieve the practically relevant threshold of 10^{-4} S cm^{-1} by tuning their structural dimensionality.

The impact of structural dimensionality on lithium-ion transport in FBHs has been probed by bond valence site energy (BVSE) calculations and ab initio molecular dynamics (AIMD) simulations. Taking Li_2FeCl_4 as an example[59–61], its orthorhombic structure is primarily composed of $FeCl_6$ octahedra and $LiCl_6$ octahedra, where lithium ions predominantly occupy octahedral sites and tetrahedral vacancies serve as intermediate states during migration. Theoretical calculations by AIMD have also revealed that ionic conduction in Li_2FeCl_4 is not a simple one-dimensional process: lithium ions migrate via octahedral–tetrahedral–octahedral hops, forming zigzag (Z-shaped) one-dimensional chains along edge-sharing polyhedra. These one-dimensional chains interweave in three-dimensional space, collectively building a connected isotropic diffusion network. We have compiled the ionic conductivities of representative FBHs in Table 1. Notably, some values already approach those of sulfide-based solid electrolytes.

In summary, the ion transport properties of FBHs are mainly influenced by crystal structure, lithium vacancy concentration, and structural dimensionality. By modulating these factors, the ion transport capability can be effectively enhanced.

Table 1. Ionic and electronic conductivity of different FBH materials.

Chemical formula	σ_{ion} (mS cm^{-1})	σ_e (mS cm^{-1})	Refs.
$FeCl_3$	/	/	[32]
$LiFeCl_4$	0.014	2.8×10^{-4}	[42]
Li_3FeCl_6	0.13	5.1×10^{-4}	[43]

$Li_{2.9}Fe_{0.9}Zr_{0.1}Cl_6$	0.25	2.2×10^{-4}	[43]
Li_2FeCl_4	0.01	2.0×10^{-4}	[59]
$Li_{3/4}Fe_{3/4}Cl_4$	0.02	1.8×10^{-6}	[60]
$Li_{1.75}FeCl_4$	0.39	1×10^{-1}	[62]
$Li_{1.3}Fe_{1.2}Cl_4$	0.22	6.9×10^{-2}	[58]
1.2LiOH-$FeCl_3$	6.1	/	[70]
$LiFeCl_3$	0.036	1.4×10^{-4}	[57]
$LiFeBr_3$	0.013	/	[57]
0.5LiF-FeOCl	0.26	/	[49]

3.2 Strategies for Enhancing Ionic Conductivity

Unlike sulfide or oxide electrolytes, FBH SSEs initially faced the challenge of insufficient intrinsic conductivity. In recent years, through a deepening understanding of structure-property relationships, researchers have developed material design strategies centered on chemical bond regulation and defect engineering. These approaches have successfully elevated the RT ionic conductivity of FBHs beyond the practical application threshold of >1 mS cm^{-1}, establishing them as strong contenders among high-performance SSEs. Crucially, these strategies focus not only on increasing the concentration of lithium-ion charge carriers but also on modulating migration energy barriers and transport pathways within the crystal lattice, thereby enabling a decisive leap in performance.

3.2.1 Self-Doping and Defect Engineering

Within the development of the FBH SSEs, a clear technological main line emerges: by systematically introducing lithium vacancies into the lattice and optimizing the topological connectivity of ion migration pathways, intrinsic breakthroughs in mixed ionic-electronic conduction are ultimately achieved at specific compositions.

Early work on Li_2FeCl_4 demonstrated the foundational principles of vacancy engineering. Prepared via high-temperature sintering of LiCl and $FeCl_3$ precursors at 673 K, Li_2FeCl_4 exhibits a RT ionic conductivity of 1×10^{-5} S cm^{-1}[42]. As shown in

Figure 2a, the resultant Li_2FeCl_4 adopts an NaCl-type superstructure with the *Cmmm* space group, in which Li^+ form a three-dimensional transport network interconnected through one-dimensional zigzag chains.

Building on this, researchers prepared $Li_{1.75}FeCl_4$ by controlling the Li/Fe ratio[60]. The adjusted composition introduced a higher concentration of lithium vacancies, resulting in a 20-fold increase in ionic conductivity (to 3.9×10^{-4} S cm^{-1}) and a remarkable four-order-of-magnitude enhancement in electronic conductivity compared to pristine Li_2FeCl_4. Structural analysis reveals that $Li_{1.75}FeCl_4$ retains the spinel structure, where Li^+ migrates from tetrahedral sites (8a) to adjacent vacant octahedral sites (16c), forming a continuous three-dimensional diffusion path. Furthermore, BVSE analysis indicates that the most favorable migration pathway in the ac plane has an energy barrier of only 0.47 eV, while the pathway in the bc plane has a barrier of 0.60 eV, collectively forming a three-dimensional network (**Figure 2b)**. This demonstrates that increasing vacancy concentration not only raises the migration rate of charge carriers but also potentially refactors the topology of migration pathways, upgrading low-dimensional channels into a three-dimensional transport network.

Pushing vacancy engineering further, the discovery of $LiFeCl_3$ achieved a vacancy concentration exceeding 33%[53]. As shown in **Figure 2c**, its cubic crystal structure features two migration pathways with energy barriers below 0.32 eV, yielding a room-temperature conductivity of approximately 3.6×10^{-5} S cm^{-1}. This finding suggests that when vacancy concentration surpasses a critical threshold, the material can spontaneously form a percolation network of low-energy-barrier channels, reducing reliance on precise engineering of a specific crystalline phase and opening new avenues for designing low-cost solid electrolytes. Recently, Sun et al. successfully prepared $Li_{1.3}Fe_{1.2}Cl_4$ by controlling the $Li^+/Fe^{2+}/Fe^{3+}$ ratio. This compound crystallizes in an orthorhombic structure with the *Cmmm* space group (**Figure 2d**)[58]. In $Li_{1.3}Fe_{1.2}Cl_4$, Fe primarily occupies the Wyckoff 2a octahedral sites, while Li and a small amount of Fe jointly occupy the Wyckoff 4f sites, forming mixed occupancy. This unique Li/Fe mixed occupancy structure not only optimizes ion transport (RT ionic conductivity of

2.28×10^{-4} S cm^{-1}) through lithium vacancies but also increases intrinsic electronic conductivity due to the mixed Fe^{2+}/Fe^{3+} valence states, creating a genuine three-dimensional mixed conduction network. For the first time, this work achieves the functional integration of ionic and electronic conduction within a single material through precise control of vacancy concentration and transition metal valence. This provides a new pathway toward simplified and high-performance battery architectures.

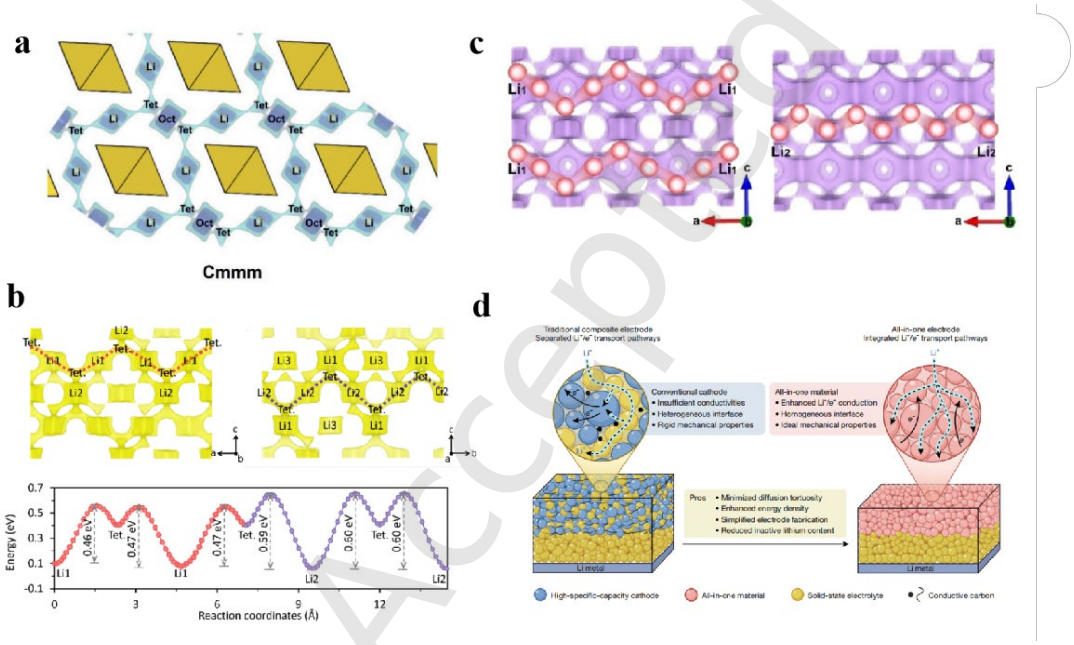

Figure 2. Lithium-ion transport pathways for different FBH SSEs. (a) Li^+ potential map calculated by BVSE superimposed with the crystal structure of Li_2FeCl_4 in the *Cmmm* space group. Reproduced with permission from Ref.[59] ©2024, American Chemical Society. (b) The Li^+ transport pathway of $LiFeCl_3$. Reproduced with permission from Ref.[60] ©2024, American Chemical Society. (c) Li^+-ion migration pathway in the ac plane (noted by the red curve) and bc plane (noted by the purple curve) in $LiFeCl_3$. Reproduced with permission from Ref.[57] ©2024,American Chemical Society. (d) The crystal schematic diagram of $Li_{1.3}Fe_{1.2}Cl_4$. Reproduced with permission from Ref.[58] ©2025, Nature.

3.2.2 Cation and Anion Substitution

Cation doping and anion substitution represent two complementary strategies for enhancing ionic conductivity in FBHs, each operating through distinct mechanisms.

Cation doping precisely introduces lithium vacancies via heterovalent substitution, enabling a stepwise increase in ionic conductivity while preserving the lattice framework. Anion substitution, in contrast, induces structural disorder that can fundamentally restructure ion transport pathways, often leading to more dramatic conductivity enhancements.

Cation doping is usually achieved by substituting higher-valence cations into the lattice; additional lithium vacancies are generated through charge compensation. For example, Zhang et al. prepared $Li_{2.9}Fe_{0.9}Zr_{0.1}Cl_6$ by doping Zr^{4+} into Li_3FeCl_6 to partially replace Fe^{3+}[43]. This heterovalent substitution introduces extra lithium vacancies while the larger Zr^{4+} ions preferentially occupy octahedral sites, stabilizing the desired *C2/m* phase and minimizing the presence of impurity phases that can impede ion transport. The combined effect yields a room-temperature ionic conductivity of 0.25 mS cm^{-1} for $Li_{2.9}Fe_{0.9}Zr_{0.1}Cl_6$, nearly double that of undoped Li_3FeCl_6 (0.13 mS cm^{-1}) (**Figure 3a**).

In contrast to cation doping, anion substitution can induce structural disorder that fundamentally breaks the constraints of traditional lattice frameworks, pushing conductivity to entirely new orders of magnitude. As shown in **Figure 3b-c**, Liu et al. reported the 1.2LiOH-$FeCl_3$ material that forms an amorphous $Fe_3O_4Cl_2$ framework through O/Cl bridging, achieving an ionic conductivity of 6.1 mS cm^{-1}[70]. This value represents an increase of more than two orders of magnitude compared to crystalline FBH. The amorphous phase provides isotropic lithium-ion migration pathways with significantly reduced diffusion energy barriers. Additionally, the presence of 12 wt% LiCl nanocrystallites within the amorphous matrix forms a synergistic transport network that further optimizes ion conduction. Similarly, the LFFOC-0.5 material (*x*LiFeOCl) employs partial F substitution for Cl to disrupt the ordered layered structure of FeOCl, forming an amorphous oxyhalide rich in Fe-O-F/Cl coordination[49]. As shown in **Figure 3d**, this mixed halogen strategy elevates the ionic conductivity to 0.26 mS cm^{-1}.

The increase of ionic conductivity in FBHs delineates a clear three-stage progression:

the first stage activates ion migration through vacancy regulation; the second stage achieves order-of-magnitude conductivity increases by optimizing vacancy concentration and structural dimensionality; and the third stage realizes intrinsic mixed conduction through the synergy of mixed occupancy and multivalence, laying the foundation for integrated electrode design.

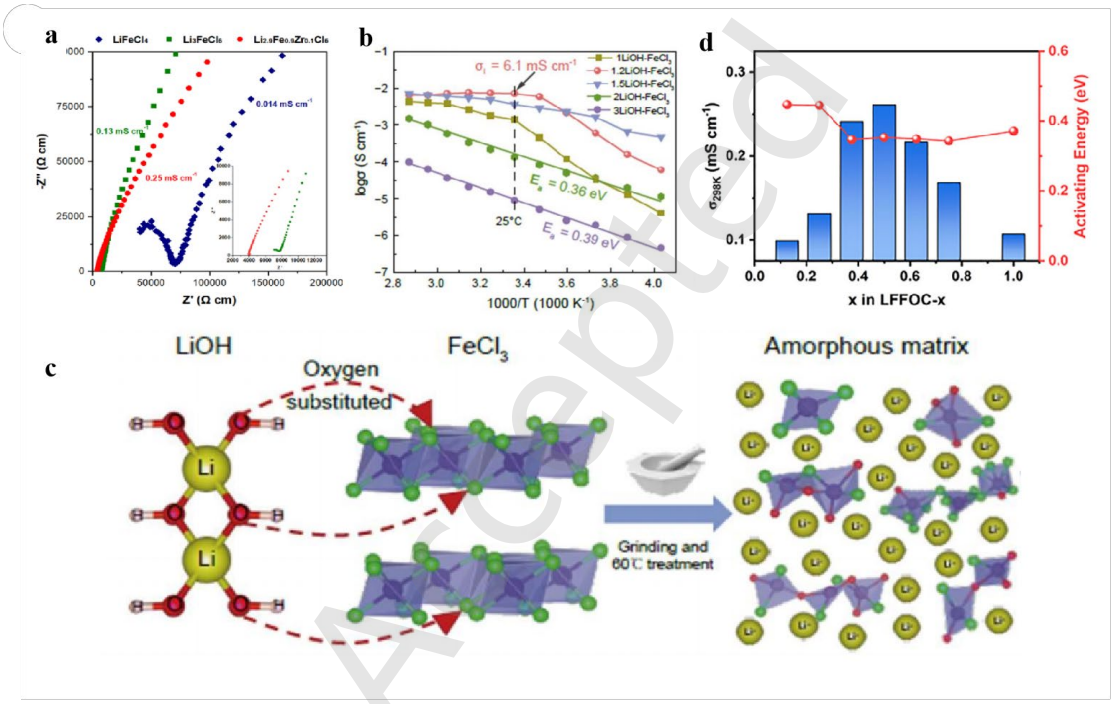

Figure 3. Summary of electrochemical data for FBH doped with different anions. (a) Nyquist plots of the as-milled $LiFeCl_4$, Li_3FeCl_6, and $Li_{2.9}Fe_{0.9}Zr_{0.1}Cl_6$ at 25 °C. Reproduced with permission from Ref.[43] ©2024, American Chemical Society. (b) Arrhenius plots of *x*LiOH-$FeCl_3$ materials (*x*=1~3) and (c) Schematic diagram of the oxygen-bridging reaction. Reproduced with permission from Ref. [70] ©2025, Oxford University Press. (d) RT-ionic conductivity and activation energy of LFFOC-*x* cathode active materials. Reproduced with permission from Ref.[49] ©2025, Wiley.

3.3 Electrochemical Stability Window and Interfacial Compatibility

In FBHs, the highest occupied molecular orbital is predominantly composed of the p orbitals of halide anions, while the lowest unoccupied molecular orbital is derived from the 3d orbitals of Fe^{3+}. This electronic configuration endows the material with excellent thermodynamic compatibility with high-voltage oxide cathodes, and its oxidation potential typically exceeds 4.0 V. This intrinsic advantage allows researchers to focus

their efforts on anode interface design and dynamic behavior studies, rather than resorting to extensive doping to ensure oxidation stability, as is necessary for sulfide systems[63].

Partial substitution of (Cl^-) with (F^-) or (Br^-) enables direct tuning of the energy levels of the anion p orbitals, while aliovalent cation substitution indirectly modulates the d orbital energy level of Fe[64]. Both strategies can broaden the electrochemical window of FBHs. Although these approaches effectively mitigate interfacial side reactions with the lithium metal anode, the underlying principle remains the identification of chemically stable components that resist reaction upon contact with the electrodes.

Another noteworthy insight into the interfacial stability arises from the brittle-to-ductile transition observed in $Li_{1.3}Fe_{1.2}Cl_4$ during charge–discharge cycling[58]. This FBH exhibits a periodic variation in mechanical properties, becoming brittle upon charging and ductile upon discharging-a feature that may allow microcracks generated during cycling to close under applied stress. The stable interface is believed not to originate from chemical inertness, but can instead stem from reversible recovery following reaction. The material retains approximately 90% of its capacity after 3000 cycles at a high rate of 5 C, suggesting that a dynamic interface enabled by intrinsic material properties may offer superior durability over the static physical contact achieved solely by mechanical pressing. Nevertheless, the relationship between the brittle-to-ductile transition and capacity retention still requires further verification. The exact mechanism of crack closure, as well as its generality across different FBHs, awaits further investigation.

Recent studies on the interface between FBHs and electrodes are progressively shifting from passive adaptation toward the exploration of dynamic regulation. The intrinsic high-voltage stability provides a foundation for simplified design, chemical substitution offers a means for interfacial tuning, and the discovery of periodic mechanical-property variations and dynamic recovery is expected to be a new direction for understanding interfacial stability.

3.4 Emerging Fe-Based Halide Electrolyte Systems

While the exploration of FBH electrolytes has traditionally focused on optimizing performance within specific crystalline frameworks through anion engineering, a fundamentally different approach has recently emerged that transcends these boundaries. “Solid-state dissociation” strategy that completely bypasses reliance on predetermined crystal lattices, pioneering an entirely new pathway to program electrolyte performance through the free combination of components[85-87]. The core of this strategy lies in the use of van der Waals crystals such as $FeCl_3$ and $ZrCl_4$ as solid solvents[88]. The metal centers (e.g., Fe^{3+}) possess strong Lewis acidity, enabling them to directly dissolve and dissociate lithium salts such as Li_2SO_4[89,90]. This process generates a homogeneous, highly ionically conductive amorphous phase in situ. Using this approach, researchers rapidly constructed a material library containing over 70 new SSEs. Notably, more than 40 of them achieved practically useful room-temperature ionic conductivity, ranging from 10^{-3} to 10^{-2} S cm^{-1}. Moreover, the approach enabled custom design of electrolytes to meet extreme operating conditions, such as ultra-high voltage (4.8 V) or low temperature (-50 °C).

This solid-phase dissociation approach represents more than an incremental improvement over conventional anion engineering. Rather than making minor adjustments within a single crystalline lattice, it establishes a novel and highly flexible amorphous material platform. This platform inherently incorporates the principles of anion engineering. For instance, this enables the direct synthesis of high-performance amorphous mixed fluorine-chlorine SSE by selecting fluorine-containing components. Moreover, the resultant high ionic conductivity and excellent interfacial contact provide a richer material foundation and greater design flexibility for developing next-generation multifunctional active electrolytes. This strategy represents a foundational, horizontally enabling paradigm that can connect and empower diverse research directions. It significantly accelerates the discovery and application of FBH SSEs tailored for specific scenarios, moving beyond the constraints of crystalline framework optimization toward a more versatile and programmable materials design approach.

4 Fe-Based Halides as Cathode Active Materials

Conventional lithium-ion batteries predominantly rely on layered oxide cathodes (e.g., $LiCoO_2$), which operate on the basis of lithium-ion intercalation and deintercalation. Their specific capacities are inherently limited by single-electron redox reactions, making it difficult to exceed the capacity ceiling of approximately 200 mAh g^{-1}. To overcome this bottleneck, researchers have turned to conversion-reaction materials that leverage multi-electron transfer. Among these, FBHs have rapidly emerged as one of the most promising cathode material families for ASSLBs, owing to their high theoretical capacity (495 mAh g^{-1}), low cost, favorable operating voltage, and unique potential for multifunctional integration. FBHs featuring high ionic conductivity and theoretical capacity can serve both as a capacity-contributing electrolyte and as a novel conversion-type cathode material. When used as a capacity-contributing electrolyte, it should exhibit excellent ionic conductivity, enabling the construction of efficient fast lithium-ion transport pathways within the composite cathode while also providing additional capacity. Furthermore, the electrolyte must possess good interfacial compatibility and structural stability, effectively suppressing adverse interfacial side reactions when in contact with oxide cathode materials. When used as a cathode material, they should possess a high theoretical capacity, a high output voltage platform and structural stability, thereby significantly enhancing the energy density of the full battery.

4.1 Fe-Based Halides with Controllable Capacity Contribution

In ASSLBs, the physical nature of solid-solid contacts introduces a set of inherent challenges that are difficult to overcome. These can be summarized into three major issues: (1) the “dead weight” problem, where inactive components contribute mass but not capacity[71-73]; (2) high ionic transport tortuosity that impedes efficient ion conduction[74-76]; and (3) unstable heterogeneous interfaces that degrade during cycling[77-79]. FBHs offer a unique solution to these challenges. The intrinsic Fe^{2+}/Fe^{3+} redox couple enables reversible reactions within the battery's operating voltage window, allowing the material to function simultaneously as both an SSE and an active material.

This enables transitioning from passive transport to active contribution.

Redox-active SSEs not only provide ionic conductivity but also deliver additional capacity, thereby significantly boosting the energy density of the composite cathode. For example, a composite cathode comprising LCO and $Li_{2.9}Fe_{0.9}Zr_{0.1}Cl_6$ (70:30 by mass) exhibits two distinct plateaus in the initial charge curve[43]. The lower plateau at 3.1 V is attributed to Fe^{2+}/Fe^{3+} oxidation in the electrolyte, while the higher plateau at 3.3 V is assigned to Co^{3+}/Co^{4+} oxidation in LCO (**Figures 4a-b**). During discharge, the electrolyte contributes a stable capacity of 26.1 mAh g^{-1}, resulting in an apparent specific capacity of 152.8 mAh g^{-1} based on LCO mass at the second discharge. This is significantly higher than previously reported LCO-based ASSLBs. The energy density calculated based on the total mass of the composite cathode reaches 399.6 Wh kg^{-1}. Notably, $Li_{1.3}Fe_{1.2}Cl_4$ possesses both high ionic conductivity (2.28×10^{-4} S cm^{-1}) and appreciable electronic conductivity (6.9×10^{-5} S cm^{-1})[58]. This enables the preparation of high-nickel NCM83 composite cathodes without the need for conductive carbon, substantially increasing the proportion of active material. As a result, the NCM83/$Li_{1.3}Fe_{1.2}Cl_4$ composite cathode with a 7:3 mass ratio reaches a discharge specific capacity of 196.1 mAh g^{-1}, with an energy density of 725.6 Wh kg^{-1}, and it also has excellent rate performance, with a reversible capacity of 100 mAh g^{-1} at 1C (**Figures 4c-d**).

The recently developed amorphous 1.2LiOH-$FeCl_3$ material exhibited stable interfacial stability under zero external pressure and excellent ionic conductivity (6.1 mS cm^{-1}) comparable to liquid electrolytes[70,80,81]. As shown in **Figures 4e-f**, when composited with LFP, the discharge capacity of LFP-1.2LiOH-$FeCl_3$ composite cathode based on LFP mass reaches 199.2 mAh g^{-1}, exceeding the theoretical capacity of LFP (170 mAh g^{-1}), and it also has excellent rate performance[82-84]. The excess capacity is attributed to the Fe^{2+}/Fe^{3+} redox reaction of the active SSEs. More notably, under zero external pressure (**Figure 4g**), the prepared LFP-1.2LiOH-$FeCl_3$ composite cathode maintains a 86.6% capacity retention after 100 cycles (**Figure 4h**).

83/LFC cell at different rates. Reproduced with permission from Ref.[47] ©2025, Nature. (e)

Charge/FBH-based active SSEs are redefining the design logic of composite cathodes. By integrating the ion transport medium and energy storage host into a single entity, they fundamentally eliminate the mass contribution of inactive components, thereby enabling a substantial leap in battery energy density.

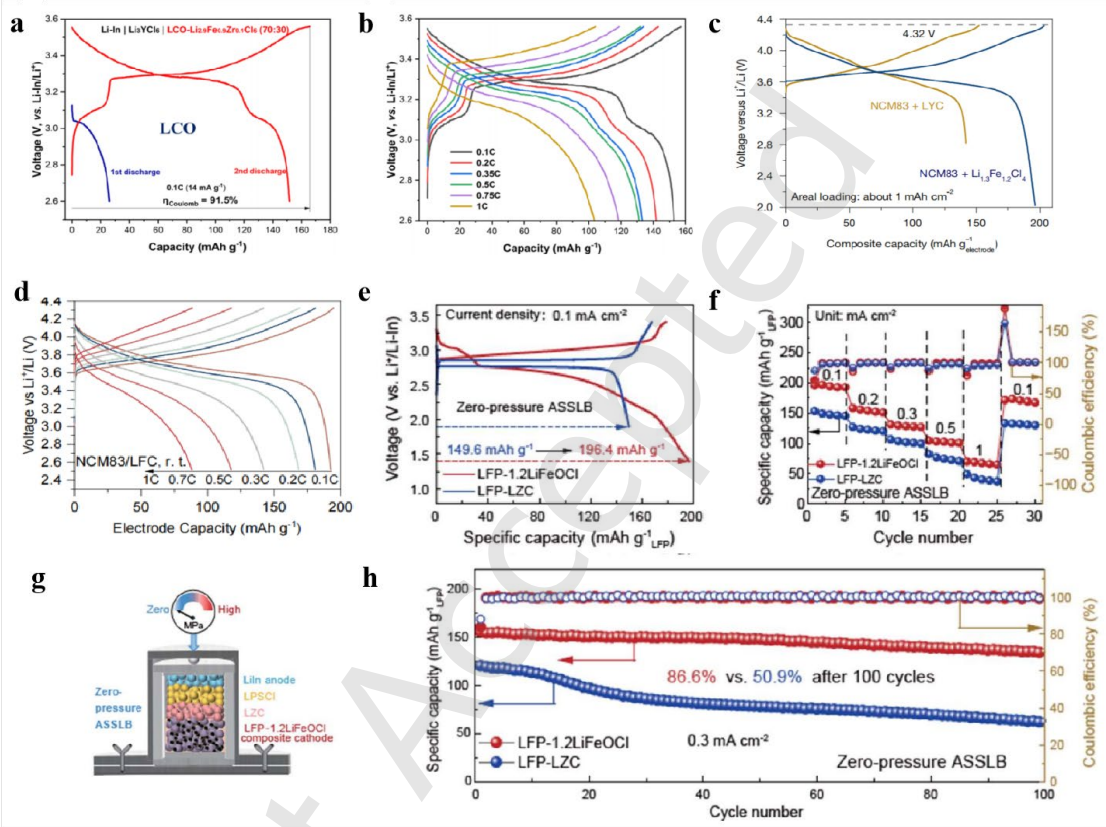

Figure 4. Application of redox-active FBHs as solid SSEs in ASSLBs. (a) The charge/discharge curves of LCO-$Li_{2.9}Fe_{0.9}Zr_{0.1}Cl_6$ composite cathode at 0.1 C and (b) rate capability at 0.1, 0.2, 0.35, 0.5, 0.75, and 1 C. Reproduced with permission from Ref.[43] ©2024, American Chemical Society. (c) The charge/discharge curves of the composite of NCM83/LYC and NCM83/$Li_{1.3}Fe_{1.2}Cl_4$ at 25 °C and 0.05 C, and (d) The charging/discharging curve of the NCMdischarge profiles of LFP-1.2LiFeOCl and LFP-LZC composite cathodes at 0.1 mA cm^{-2}, and (f) The rate performance of LFP-1.2LiFeOCl and LFP-LZC composite cathodes, and (g) Schematic diagram of the zero-pressure ASSLB configuration and (h) cycling stability of LFP-1.2LiFeOCl and LFP-LZC composite cathodes at 0.3 mA cm^{-2}. Reproduced with permission from Ref. [70] ©2025, Oxford University Press.

4.2 Reaction Mechanisms: From Intercalation to Conversion

The core breakthrough of FBH cathodes lies in their unique intercalation-conversion coupled reaction mechanism. This mechanism is not a simple superposition of intercalation and conversion reactions but rather, through sophisticated crystal structure design, enables the framework stability provided by the intercalation reaction and the multi-electron transfer capability endowed by the conversion reaction to work synergistically within the same material system. This synergy achieves high capacity approaching the theoretical limit while maintaining good reaction reversibility, establishing a new design paradigm for overcoming the capacity bottlenecks of traditional cathode materials.

A representative example of this coupled mechanism is demonstrated by the $LiFeCl_3$ cathode. As shown in **Figures 5a-b**, the $LiFeCl_3$ cathode exhibits an initial discharge capacity of 446 mAh g^{-1} at 0.1 mA cm^{-2}[57], reaching 94% of the theoretical capacity (475 mAh g^{-1}) based on three electron transfer. Its charge-discharge curves display three characteristic plateaus. The plateau at approximately 3.7 V corresponds to the intercalation reaction involving one-electron transfer (contributing approximately 150 mAh g^{-1}), while the plateau at approximately 1.5 V originates from the conversion reaction involving two-electron transfer (contributing approximately 300 mAh g^{-1}). The dQ/dV further reveals four charging peaks and three discharging peaks within the range of 1.0-3.9 V, corresponding to multistep reversible redox transformations between Fe^{3+} and Fe^0 (**Figure 5c**). Even at a high current density of 1.0 mA cm^{-2}, $LiFeCl_3$ maintains a specific discharge capacity of 202 mAh g^{-1}, highlighting the critical role of high ionic conductivity in supporting reaction kinetics. As shown in **Figure 5d**, after 100 cycles at 0.3 mA cm^{-2}, the $LiFeCl_3$ cathode delivers a discharge capacity of 240 mAh g^{-1}, with a capacity retention rate of 73%, confirming the good reversibility of the intercalation-conversion coupled process. The versatility of this coupled mechanism across different compositions is further illustrated by the LFFOC-0.5 material (0.5LiF-FeOCl), prepared by partially substituting (Cl^-) with (F^-)[49]. This material achieves a discharge specific capacity of 201 mAh g^{-1} at 0.5 mA cm^{-2} and maintains over 100 mAh g^{-1} at 2.0 mA cm^{-2}, corresponding to a power density of 1846 W kg^{-1} (**Figures 5e-f**). After 700

cycles, the capacity retention of the LFFOC-0.5-based ASSLBs reaches 65% (**Figure 5i**), a benefit attributed to the intimate electrode/electrolyte interface enabled by the SSE's high compressibility[91].

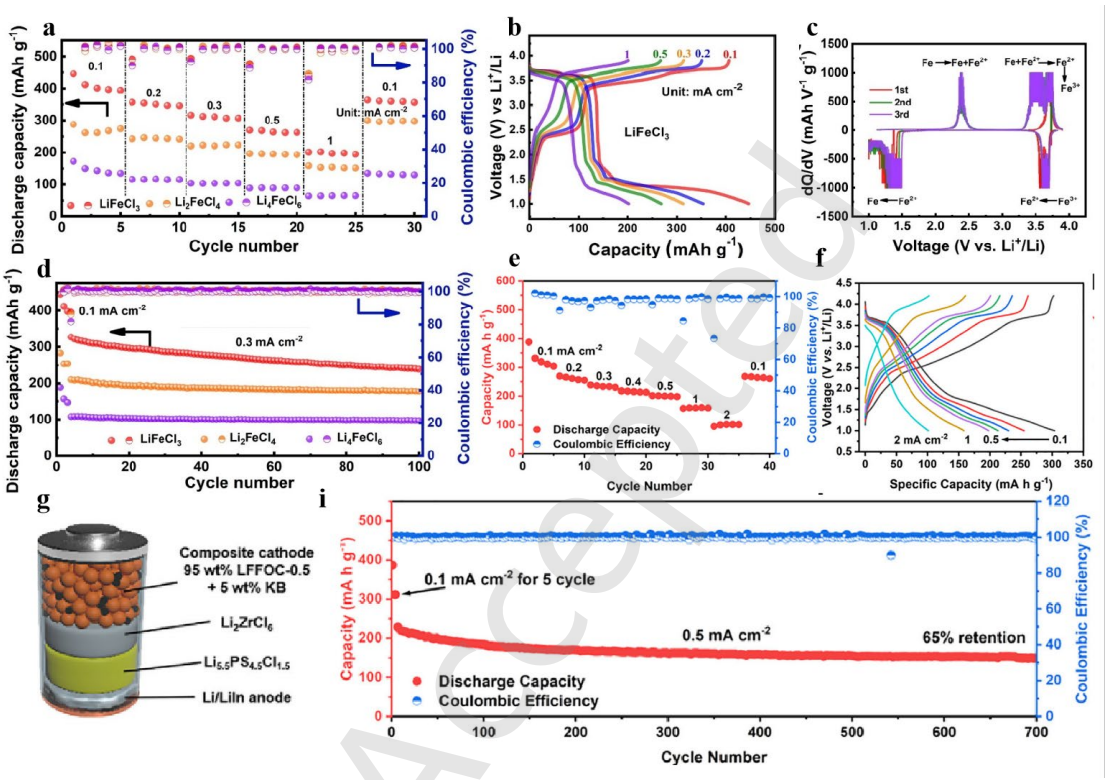

Figure 5. Application of redox-active FBH compounds as positive electrodes in ASSLBs. (a) Rate performance of Li_xFeCl_{x+2} cathode materials at various current densities of 0.1-1 mA cm^{-2}, and (b) charging-discharging profiles of $LiFeCl_3$ cathode material at various current densities, and (c) dQ/dV curve of the $LiFeCl_3$ cathode material in the voltage window of 1–3.9 V at 0.1 mA cm^{-2}, and (d) cycling performance of Li_xFeCl_{x+2} cathode materials at 0.3 mAcm^{-2} after activation at 0.1 mAcm^{-2} for 3 cycles. Reproduced with permission from Ref.[57] ©2025, Wiley. (e-f) Rate performance and charging-discharging profiles of LFFOC-0.5 CAM at various current densities from 0.1 to 2 mA cm^{-2}, 25 °C, and (g) schematic illustration of the assembled ASSLB using LFFOC-0.5 CAM, and (i) long-term cycling performance of LFFOC-0.5 CAM with LiIn anode at 0.5 mA cm^{-2} with 5 cycles activation at 0.1 mA cm^{-2} and 25 °C. Reproduced with permission from Ref.[49] ©2025, Wiley.

The mechanistic underpinnings of this coupled reaction have been systematically elucidated through structural and spectroscopic analyses. A detailed exploration of the

energy storage mechanism of $LiFeCl_3$ is provided by Zhou et al[57]. As shown in **Figures 6a-c**, in situ XRD of $LiFeCl_3$ shows that (101) and (220) diffraction peaks shift to higher angles during charging, with the lattice spacing contracting from 6.0 Å to 5.8 Å, corresponding to framework contraction caused by Li^+ extraction. The peak positions recover in the early stage of discharge, confirming the full reversibility of the intercalation reaction. When discharged to below 1.37 V, the characteristic peaks of $LiFeCl_3$ gradually weaken, while the (111) and (311) diffraction peaks of LiCl appear and sharpen. Transmission electron microscopy reveals that the cubic LiCl phase (lattice spacing 2.6 Å) gradually replaces the pristine phase (**Figure 6d**). Upon full discharge to 1.0 V, the $LiFeCl_3$ peaks completely disappear, and a broadened peak assigned to Fe (110) emerges, indicating the formation of amorphous Fe. X-ray absorption near-edge structure (XANES) analysis shown in **Figures 6e-i** further tracks the evolution of the Fe valence state. During discharge, Fe^{3+} is progressively reduced to Fe^{2+} at 1.7 V, followed by the emergence of mixed Fe^0/Fe^{2+} characteristics upon further discharge to 1.0 V. Ultimately, the initial valence state is fully and reversibly recovered during the subsequent charging process. These results collectively delineate a coupled reaction pathway. In the first (intercalation) stage, the Fe^{3+}/Fe^{2+} redox couple is active, governed by reversible lattice expansion/contraction. In the subsequent (conversion) stage, Fe^{2+} is further reduced to Fe^0 with concomitant LiCl formation. Critically, the interfacial processes in both stages are reversible.[92-94].

The core value of the intercalation-conversion coupled mechanism of Li_xFeCl_{x+2} lies in its synergistic enhancement. During the intercalation reaction stage, the Fe-Cl framework remains intact, providing a structural template for the subsequent conversion reaction and avoiding the drastic volume changes and structural collapse that can result from direct conversion. During the conversion reaction stage, multi-electron transfer releases high capacity, while the ion transport channels established during the intercalation stage ensure favorable reaction kinetics. Although intercalation-conversion occurs at distinct voltage ranges (intercalation plateau at ~3.7 V, conversion plateau at ~1.5 V), these two stages are seamlessly connected in terms of structural

evolution, collectively endowing FBH cathodes with both high capacity and long cycle life. Other compounds in the Li_xFeCl_{x+2} series, such as Li_2FeCl_4 and Li_4FeCl_6, also exhibit coupled electrochemical behavior[50,95,96]. However, their higher molecular weights and lower ionic conductivities result in inferior capacity and rate performance compared to $LiFeCl_3$, suggesting that future efforts are expected optimize intrinsic transport properties while maintaining the coupling mechanism.

The intercalation-conversion coupled mechanism represents the main effective strategy for achieving high energy density for FBH cathodes. By merging the advantages of both reaction types, it breaks through the capacity ceiling of single-reaction mechanisms while ensuring stable cycle life through reversible structural evolution.

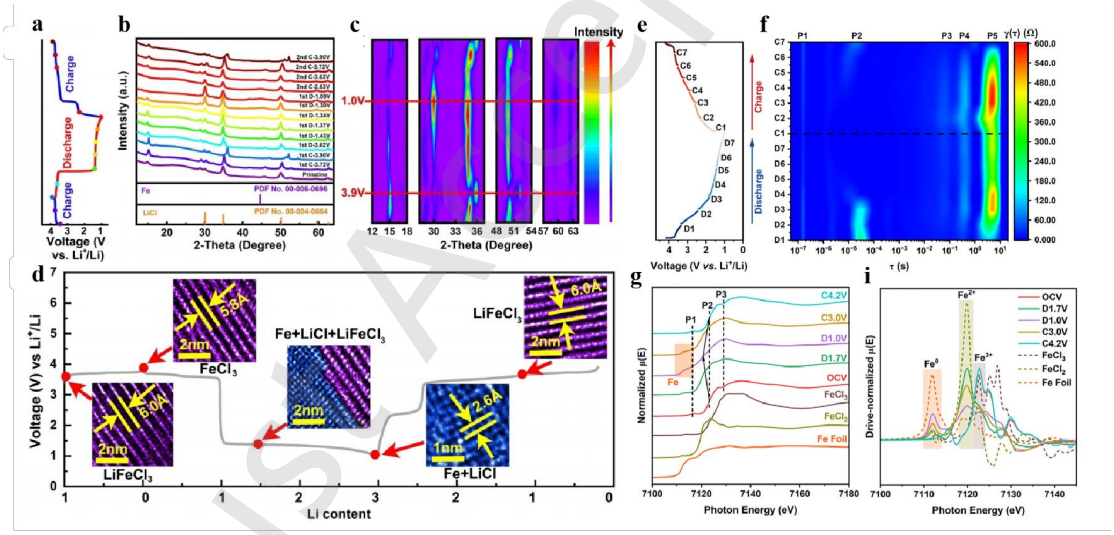

Figure 6. Structural changes of redox-active FBH cathodes during charge–discharge processes. (a) Charge-discharge profiles, (b-c) ex situ XRD patterns during the charging-discharging process, and (d) TEM images of $LiFeCl_3$ cathode material at different charging-discharging depths. Reproduced with permission from Ref.[57] ©2025, Wiley. (e-f) Quasi-situ EIS and the corresponding DRT analysis of LFFOC-0.5 CAM after the first cycle, and (g-i) normalized Fe K-edge XANES spectra and the first derivative of the XANES spectra of LFFOC-0.5 CAM at different charging–discharging depths. Reproduced with permission from Ref.[49] ©2025, Wiley.

4.3 High-Capacity Conversion Cathode: The Case of $FeCl_3$ and FeF_3

As a typical representative of conversion-type FBH cathodes, one of the advantages of $FeCl_3$ lies in challenging the conventional perception that conversion reactions are confined to low voltage ranges. Leveraging the unique thermodynamic environment of the Fe^{3+}/Fe^{2+} and Fe^{2+}/Fe^0 redox couples within the halide matrix, $FeCl_3$ achieves a flat discharge plateau as high as 3.5-3.8 V (vs. Li^+/Li) while delivering capacity (495 mAh g^{-1}) approaching the theoretical limit through three-electron transfer. This synergy between high voltage and multi-electron transfer enables $FeCl_3$ to exhibit energy density comparable to intercalation cathodes while maintaining an extremely low cost advantage.

The electrochemical behavior of $FeCl_3$ is characterized by highly reversible two-step redox reactions. During discharging, cathodic peaks appear at 3.56 V and 3.67 V; upon charging, the corresponding anodic peaks are observed at 3.70 V and 3.74 V (**Figure 7a**)[32]. The peak positions exhibit only minor shifts in subsequent cycles, indicating high reaction reversibility. The unusually high conversion voltage of $FeCl_3$ originates from the Fe-Cl bonds[33]. The strong electronegativity of the halogen anions endows the Fe^{3+}/Fe^{2+} and Fe^{2+}/Fe^0 redox couples with relatively high redox potentials relative to metallic lithium, while the high enthalpy of formation of the conversion product LiCl further contributes to the reaction driving force. This mechanism of synergy between bonding and formation enthalpy provides theoretical guidance for developing other high-voltage conversion-type cathode materials. Notably, $FeCl_3$ demonstrates excellent electrochemical performance. After 1000 cycles at 0.5 C and room temperature, the capacity retention of $FeCl_3$ reaches 83%, with an average Coulombic efficiency of 99.98% (**Figure 7b**).

The SSE plays a critical role in unlocking the full performance potential of $FeCl_3$. When paired with the $Li_2ZrCl_{5.6}F_{0.4}$ (LZCF) solid electrolyte, $FeCl_3$ delivers capacities of 440, 401, and 367 mAh g^{-1} at current densities of 0.1, 0.15, and 0.25 A g^{-1}, respectively (**Figure 7c**)[33]. Even at a high current density of 0.5 A g^{-1}, it maintains a capacity of 314 mAh g^{-1}, significantly outperforming the reference system. As shown in **Figure 7d**, after 500 cycles at a high current density of 1.0 A g^{-1}, $FeCl_3$ in the LZCF

system still retains a capacity of 213 mAh g^{-1}, with a retention rate as high as 84%. Overall, the capacity, rate capability, and cycling stability of $FeCl_3$ are significantly superior to those of Li_2ZrCl_6. This difference originates from the superior interfacial compatibility and ion transport matching between LZCF and $FeCl_3$, suggesting that future practical development should optimize the cathode material and electrolyte as a coupled system. Collectively, these results demonstrate that $FeCl_3$ achieves exceptional cycling reversibility in the three-electron transfer.

Mechanistic investigations further elucidate the structural evolution underpinning this reversibility. As shown in **Figures 7e-f**, ex situ XANES tracking of the Fe valence state evolution confirms the high reversibility of the Fe^{3+}/Fe^{2+} redox couple[21]. Energy-dispersive X-ray diffraction (EDXRD) reveals a multistep phase transformation process of $FeCl_3$ during the first cycle (**Figures 7g-i**). In the early stage of discharge, the pristine $FeCl_3$ phase diminishes, and an intermediate α-phase (space group $P6_3cm$) appears. Further lithiation leads to the transformation of the α-phase into a lithium-rich β-phase. The charging process does not follow a simple reverse path but instead proceeds through a solid-solution delithiation region to form a γ-phase, followed by recovery through a second solid-solution region. Although the structural evolution of $FeCl_3$ is not directly reversible in a strict sense, overall electrochemical reversibility is achieved through multistep phase transition pathways.

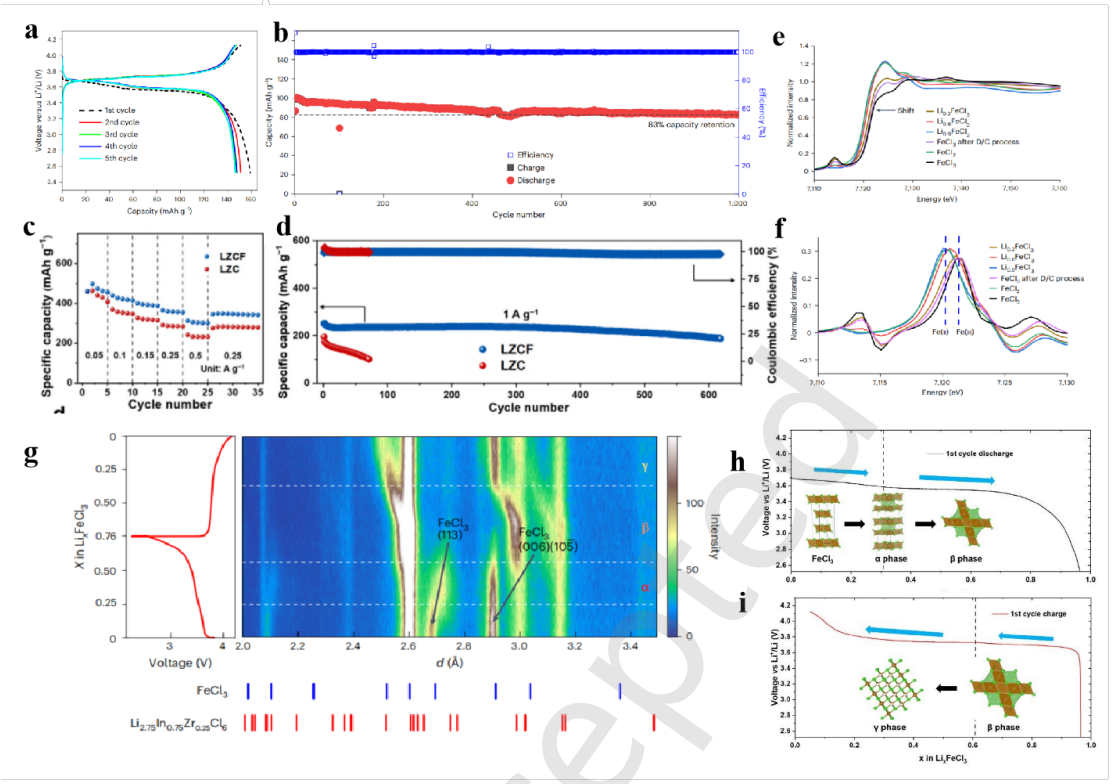

Figure 7. The performance of $FeCl_3$ as the cathode in the ASSLBs, and its structural changes during charging and discharging. (a) Charge/discharge profile of $FeCl_3$ at 0.1 C and RT with $Li_3YCl_3Br_3$ electrolyte, and (b) long-term cycling performance at 0.5 C and RT. Reproduced with permission from Ref.[32] ©2024, Nature. (c) Rate capability for $FeCl_3$ cathode in LZCF and LZC SSEs, and (d) cycling performance at 1 A g^{-1} in the potential range of 1.5-3.9 V. Reproduced with permission from Ref.[33] ©2024, Wiley. (e) Ex situ Fe K-edge XANES spectra of $FeCl_3$ at different charge/discharge states, and (f) first-order derivatives of Fe K-edge XANES spectra of $FeCl_3$ at different charge and discharge states, and (g) contour map between 2 and 3.5 Å of the phase evolution of the cathode during the initial discharging and charging processes, and (h-i) structure evolution diagram of $FeCl_3$ during the charge-discharge process. Reproduced with permission from Ref.[32] ©2024, Nature.

In addition, other FBHs have been reported to be explored for solid-state batteries. For instance, FeF_3 can serve as a novel conversion-type cathode owing to its excellent high specific capacity (712 mAh g^{-1}) and high-voltage stability. During the charge/discharge of FeF_3, a multi-electron transfer proceeds in two successive stages: the first involves the conversion from Fe^{3+} to Fe^{2+}, and the second from Fe^{2+} to Fe (**Figures 8a,d).** Two pairs of voltage plateaus of the discharge–charge curve can be

ascribed to the reversible conversion reactions between FeF_3/Li^+ and Fe/LiF associated with the lithiation/delithiation process, matching well with the redox peaks in the cyclic voltammogram (CV) curves. The first discharge curve shows a plateau at ~3 V, indicating that the Fe^{3+} from FeF_3 is gradually reduced to Fe^{2+} during Li intercalation ($Li^+ + e^- + FeF_3 \rightarrow LiFeF_3$). The second plateau at lower potential corresponds to the conversion reaction ($2Li^+ + 2e^- + LiFeF_3 \rightarrow 3LiF + Fe$)[97,98]. The lower and longer plateau observed during the first discharge may be respectively attributed to the initial overpotential often observed in conversion reactions for the lithiation of the slightly fluorinated carbon and the formation of cathode solid electrolyte interphase. The voltage profiles of different rates demonstrate similar loops with typical redox plateaus, suggesting good reversibility and favorable rate capability (**Figure 8b-c**). Thus, FeF_3 is widely regarded as one of the candidates for solid-state batttteries.

As a low-cost conversion-type cathode, $FeCl_3$ redefines the application boundaries of conversion reactions through the trinity of high voltage plateau, multi-electron transfer, and long cycle life. Its exceptional performance, demonstrated in the $Li_2ZrCl_{5.6}F_{0.4}$ electrolyte, further reveals the critical role of cathode-electrolyte interfacial synergy in achieving performance leaps. Future research can deepen the understanding and control of multistep phase transformation pathways and explore the compatibility of $FeCl_3$ and FeF_3 with a broader range of electrolytes to fully unleash its practical potential.

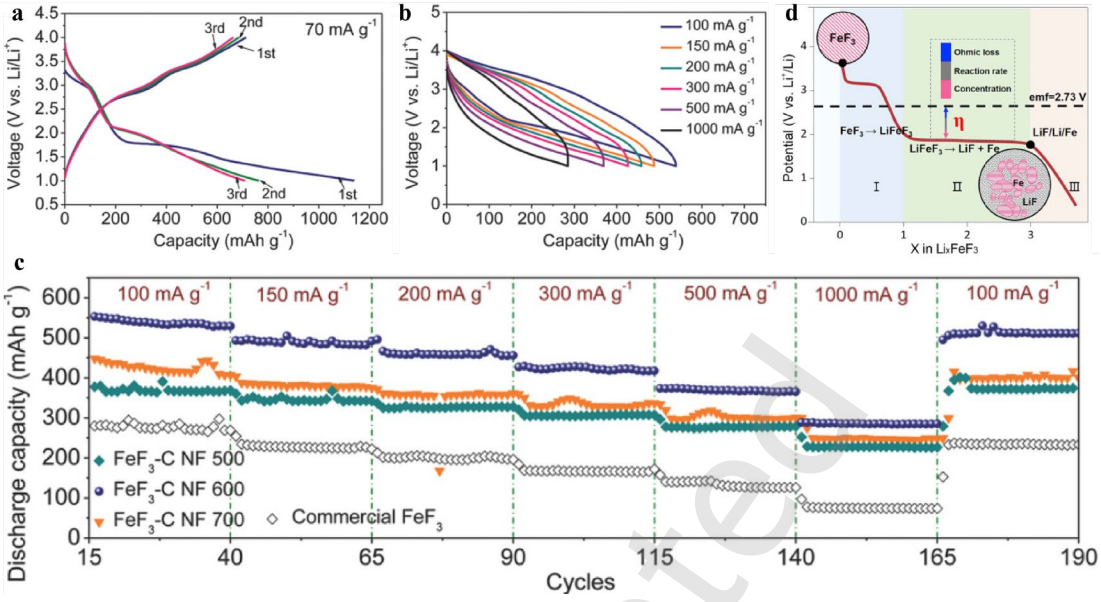

Figure 8. The performance of FeF_3 as the cathode in the ASSLBs. (a) Galvanostatic discharge/charge curves of the FeF_3-C NF 600 electrode at a current density of 70 mA g^{-1} with a voltage range of 1-4 V (vs Li/Li^+), and (b) voltage profiles of the FeF_3-C NF 600 electrode at various current densities (100-1000 mA g^{-1}),and (c) rate capability of the FeF_3-C NF samples (500, 600, 700) in comparison with that of commercial FeF_3 nanoparticles (ball-milled with C additives; at the same or higher total C content in the electrode) at different current densities. Reproduced with permission from Ref.[97] ©2018, Wiley. (d) The Phase Reactions and Hysteresis of the FeF_3 Cathode in Lithium Batteries. Reproduced with permission from Ref.[98] ©2019, Elsevier.

4.4 The All-in-One Cathode: Integrating Active Material, Electrolyte, and Conductive Agent

The composite cathode of traditional ASSLBs has long been constrained by the three-component paradigm, in which active materials contribute capacity, solid electrolytes facilitate ion transport, and conductive carbon enables electron conduction. The latter two components, as non-capacity-contributing "dead weight," not only dilute electrode energy density but also introduce complex multiphase interface issues that compromise stability and performance.

A transformative departure from this paradigm is exemplified by the $Li_{1.3}Fe_{1.2}Cl_4$

material, which achieves an integrated design through its intrinsic high mixed ionic-electronic conductivity (~10^{-5} S cm^{-1})[58]. The designed $Li_{1.3}Fe_{1.2}Cl_4$ integrates the three functions of active material, electrolyte, and conductive agent into a single entity, fundamentally eliminating the mass contribution of inactive components. Beyond this compositional integration, the material's exceptional electrochemical performance is underpinned by a dynamic and reversible iron migration mechanism. This mechanism also highlights the structural self-adaptability during cycling, enabling the electrode to accommodate volume changes and maintain stable ion and electron transport pathways over extended operation.

Various advanced techniques have been employed to study the three-dimensional ion transport mechanism of $Li_{1.3}Fe_{1.2}Cl_4$. The crystal structure was subsequently characterized by combined X-ray diffraction (XRD), neutron diffraction and pair distribution function (PDF) analyses, which identified a *Cmmm* space group (**Figures 9a-c**). More specifically, the Li and Fe atoms are bonded to six Cl atoms to form edge-sharing octahedra (**Figure 1g**). Most of the Fe atoms sit in Wyckoff position 2a, whereas Li atoms and a small amount of Fe atoms occupy Wyckoff position 4*f*. The Li^+ diffusion dynamics of $Li_{1.3}Fe_{1.2}Cl_4$ revealed by ab initio molecular dynamics (AIMD) simulations (**Figure 9e**) show that the Li^+ forms a fast three-dimensional diffusion network for fast ion transport, resulting in high ionic conductivity (0.22 mS cm^{-1}).

Ex situ X-ray absorption near-edge structure (XANES) and X-ray diffraction (XRD) techniques have confirmed the highly stable structure of $Li_{1.3}Fe_{1.2}Cl_4$ during charge–discharge, with a volume change of only 8%. The Cl and Fe K-edge XANES spectra have revealed the electron transfer process during the charge-discharge process (**Figure 9g-i**). Upon charging, Fe^{2+} is completely oxidized to Fe^{3+}, as evidenced by a progressive shift of the Fe K-edge (E_0) to higher energy. This oxidation was fully reversed during discharge, with Fe^{3+} subsequently reducing to Fe^{2+}. Notably, the generation of Fe^{3+} coincides with the transition from insulating to conductive behaviour, consistent with conductivity measurements (**Figure 9k**). Ex situ XRD measurement revealed two phase transitions during the discharge of $Li_{1.3}Fe_{1.2}Cl_4$ (**Figure 9j)**, which is consistent with the

two charge–discharge plateaus. Rietveld refinement of the XRD data indicates an overall volume change of approximately 8.0% between the fully discharged and charged states. These characterization demonstrate that $Li_{1.3}Fe_{1.2}Cl_4$ exhibits good reversibility of Li^+ intercalation and deintercalation during charge–discharge.

Probing the change of ionic and electronic conductivities during the charge-discharge process is very important to evaluate the possible use of FBHs as redox-active electrolytes. For example, the intermediate products of $Li_{1.3}Fe_{1.2}Cl_4$ during charge–discharge were prepared by electrochemical and ball-milling methods to study the evolution of their ionic and electronic conductivities. In situ Electrochemical impedance spectroscopy (EIS) was also explored to elucidate cathode dynamics during Li^+ intercalation/deintercalation at room temperature (**Figure 9f**) and 60 °C. The EIS measurement indicated that their ionic and electronic conductivities change very little and remain at a relatively high level (generally $>10^{-5}$ S cm^{-1}) during the charge–discharge process (**Figure 9l**), indicating excellent kinetic stability. This explains why $Li_xFe_{1.2}Cl_4$ can be used as an "integrated positive electrode"[58].

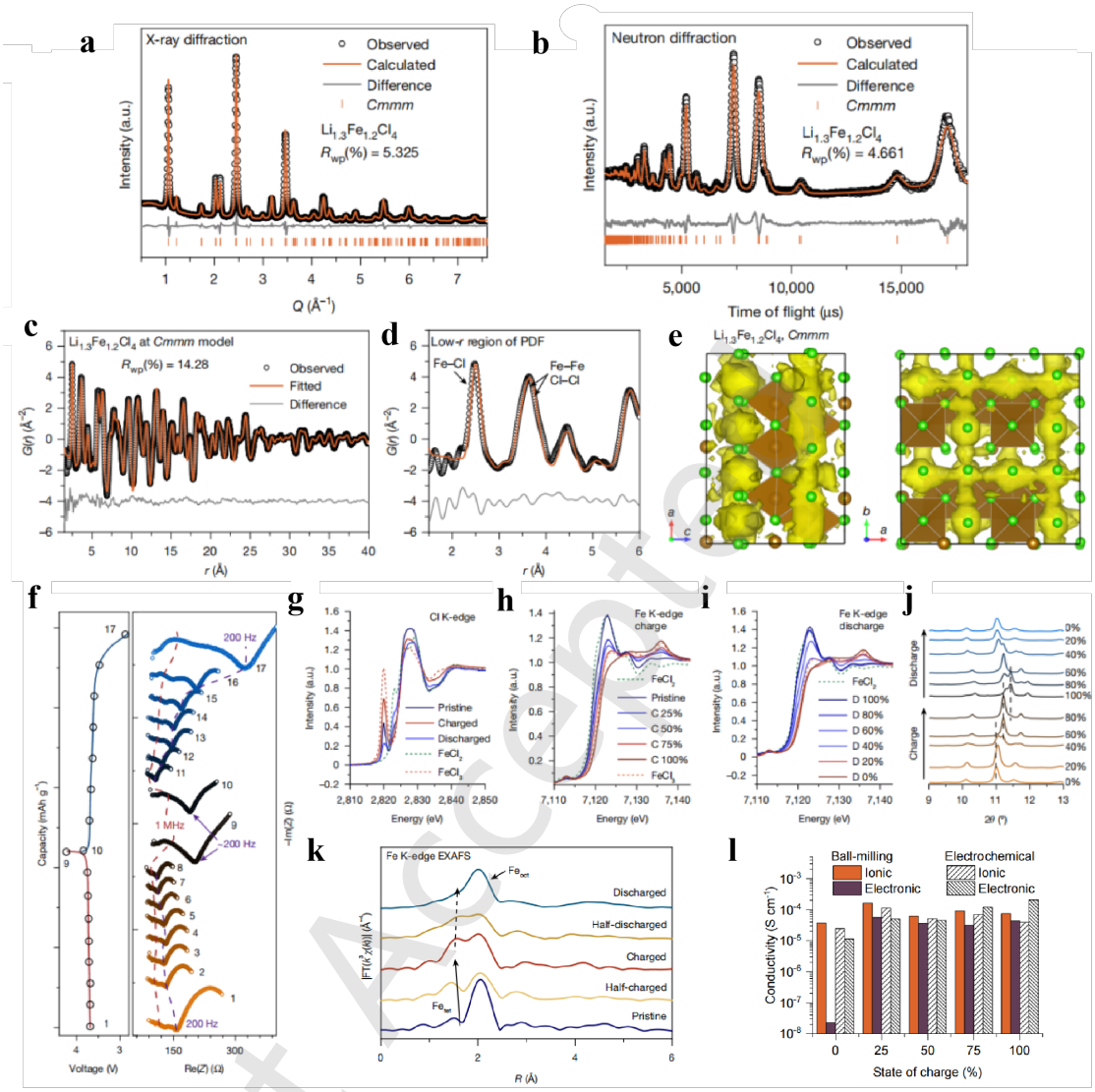

Figure 9. Charge/discharge mechanism of $Li_xFe_{1.2}Cl_4$ halide framework. (a,b) Synchrotron-based XRD (a) and neutron diffraction (b) patterns with the Rietveld refinement results for $Li_{1.3}Fe_{1.2}Cl_4$ as a function of momentum transfer (Q). The weighted profile residual (R_{wp}) of the fittings is also presented and (c) the reduced PDF, G(r), and the fitted result for $Li_{1.3}Fe_{1.2}Cl_4$ as a function of interatomic distance r. The difference is offset by -4 for clarity and (d) the G(r) in the low-r region for $Li_{1.3}Fe_{1.2}Cl_4$ and (e) Li^+ probability density marked by yellow isosurfaces from AIMD simulations at 900 K in Cmmm-phase $Li_{1.25}Fe_{1.25}Cl_4$ and (f) in situ EIS of $Li_{1.3}Fe_{1.2}Cl_4$ cell. Data sets 1-9 correspond to the charging process, measured at 15 mAh g^{-1} intervals; data sets 10-17 represent the discharging process, measured at 20 mAh g^{-1} intervals and (g) the Cl K-edge XANES spectra of pristine, fully charged and fully discharged $Li_{1.3}Fe_{1.2}Cl_4$ and (h-j) ex situ Fe K-edge

XANES spectra (h,i) and ex situ XRD profile as a function of Bragg angle (θ) with an X-ray wavelength of 0.3497 Å (k) of $Li_{1.3}Fe_{1.2}Cl_4$ at different states of charge and discharge and (k) Fourier transform (FT) of the Fe K-edge EXAFS oscillation function $\chi^{(k)}$ of charged and discharged $Li_{1.3}Fe_{1.2}Cl_4$ as a function of radial distance R, with a k^3 weighting and (l) Graph showing the changes in ionic conductivity and electronic conductivity during the charging and discharging process of $Li_{1.3}Fe_{1.2}Cl_4$. Reproduced with permission from Ref.[58] ©2025, Nature.

5. Conclusion and Outlook

In summary, Fe-based halides (FBHs) leverage the dual advantages of high elemental abundance and low cost, and through structural design have exhibited novel functionalities such as mixed ionic/electronic conductivity and dynamic self-healing, making them a material system with unique potential for all-solid-state lithium batteries (ASSLBs). At the same time, it should be objectively recognized that these advantages are currently based primarily on laboratory-stage validation. The proposed integrated interface design strategies still require further verification under practically relevant conditions (e.g., high areal capacity, low stack pressure, and wide-temperature operation). A gap remains between the fundamental understanding already achieved and the stringent requirements of practical cells, and this gap needs to be systematically addressed. Future in-depth exploration of the following key issues will, to a large extent, determine whether FBHs can evolve from promising material candidates into truly viable technological solutions.

(1) Accelerating Discovery through High-Throughput Approaches: The vast compositional and structural space of FBH renders traditional trial-and-error methods inefficient. By integrating first-principles calculations, molecular dynamics simulations, and machine learning, structure-property relationship models can be established to link material composition and structure with key performance metrics such as ionic conductivity, voltage, and stability. This enables virtual high-throughput screening of new candidates, accelerating the discovery of high-performance materials while providing deep insights into microscopic mechanisms. Such an approach serves as a critical bridge connecting fundamental research with applied development.

(2) Interfacial Stability with Lithium Metal Anodes: The thermodynamic instability of most FBHs electrolytes against metallic lithium is one of the primary obstacles to realizing their high-energy-density potential. The commonly envisioned strategy of forming a dense, uniform, and ionically conductive solid electrolyte interphase to passivate subsequent side reactions is sound in principle, yet its practical implementation requires satisfying multiple, often mutually constraining criteria: negligible electronic conductivity to prevent continued electrolyte reduction, sufficiently high ionic conductivity to control interfacial impedance, good mechanical compliance to accommodate lithium volume changes, and chemical stability over long-term cycling. Recent concepts such as valence-gradient layers incorporating iron nanoparticles (Fe^0, Fe^{2+}, Fe^{3+}) demonstrate the promise of proactive interface design, but their long-term structural and chemical evolution under current load and temperature gradients remains poorly understood. Whether the interphase can achieve truly self-limiting growth, rather than gradually evolving into an electronically leaky, high-impedance layer, still requires careful observation and thorough verification. Future research may increasingly employ in situ characterization techniques to track dynamic interfacial evolution and, on this basis, design gradient structures capable of self-terminating growth.

(3) Balancing Energy Density and Power Density: In conventional composite cathodes, substantial amounts of SSEs and conductive additives are required to establish ion and electron transport pathways, directly compromising energy density. While all-in-one cathode materials such as $Li_xFe_{1.2}Cl_4$ fundamentally address this issue by integrating all three functions into a single phase, further optimization is needed to balance specific capacity, ionic conductivity, and electronic conductivity. Excessively high electronic conductivity or superhigh ionic conductivity may limit rate capability. Moreover, for high-capacity conversion materials like FeF_3, significant volume changes and sluggish kinetics remain major obstacles. Future material discovery should therefore move beyond simple elemental substitution toward crystal structure innovation and multi-anion engineering. Unique frameworks such as pyrochlore-like

structures, which may support single-phase lithiation mechanisms that mitigate volume strain, warrant further investigation. Systematic exploration of multi-anion combinations (F, Cl, Br, O) offers a pathway to tailor materials that simultaneously achieve high stability, high conductivity, and suitable mechanical properties.

(4) Air Stability and Scalable Preparation: The air-stability advantage of FBHs over sulfides is often regarded as a significant manufacturing benefit, but this merits a comprehensive assessment. Currently, typical compositions, upon exposure to ambient moisture, may still undergo irreversible hydrolysis, accompanied by the generation of acidic gases, structural degradation, and permanent loss of ionic conductivity. Consequently, multiple steps from synthesis and storage to electrode fabrication and cell assembly still largely rely on strict inert-atmosphere control, meaning that the cost advantage conferred by air stability has yet to be fully realized. Partial fluorine substitution to enhance moisture tolerance is a direction receiving considerable attention; however, this approach often entails a trade-off with reduced ionic conductivity and material deformability, and the associated property compromises still lack systematic understanding. Moreover, while mechanochemical methods are flexible at the laboratory scale, substantial room for improvement remains in terms of batch-to-batch reproducibility, impurity control, and energy efficiency when transitioning to large-scale production. Future research may focus on constructing a multi-objective parameter space that comprehensively considers moisture tolerance, processability, and electrochemical performance, coupled with life-cycle analysis and techno-economic assessment, to more holistically evaluate the practical industrialization prospects of FBHs.

Through sustained and prudent efforts in the above key directions, FBHs are expected to progressively move from laboratory highlights toward industrial-grade applications, providing critical material support for the development of safe, high-energy-density all-solid-state lithium batteries, and thereby making tangible contributions to the sustainable development of global energy storage technologies.

Acknowledgements

None.

Author contribution statement

Chonggui Lei is responsible for Conceptualization, Data curation, Writing – original draft and Writing – review & editing. Zuxin Long is responsible for Writing – review & editing. Lang Yuan is responsible for Writing – review & editing. Liansheng Li is responsible for Funding acquisition, Supervision and Writing – review & editing. Geng Li is responsible for Supervision and Writing – review & editing. Yu Lu is responsible for Writing – review & editing. Qinghua Liang is responsible for Funding acquisition, Supervision and Writing – review & editing. All the authors have approved the final manuscript.

Data availability

Not applicable.

Declaration of competing interest

All the contributing authors report no conflicts of interest in this work.

Funding

The authors acknowledge the financial support from the National Natural Science Foundation of China (Grant Nos. 52572053 and 52504342), the Department of Science and Technology of Jiangxi Province (Grant No. gpyc20240079), Natural Science Foundation of Jiangxi province (20232ACB214001), key Laboratory of Rare Earths, Chinese Academy of Sciences (Grant No. E32PF00116). The authors also thank the financial support from the Chinese Academy of Sciences and the Jiangxi Province Human Resources and Social Security Department.

Use of AI statement

None.

References

[1] P.U. Nzereogu, A. Oyesanya, S.N. Ogba, et al., “Solid-State lithium-ion battery electrolytes: Revolutionizing energy density and safety” Hybrid Adv. 8 (2025) 100339.

[2] H. Huo, J. Janek, "Solid-State Batteries: From 'All-Solid' to 'Almost-Solid'," Natl. Sci. Rev. 10 (2023): nwad098.

[3] H. Huang, R. Guo, Y. Li, C. Dang, et al., "Electrolyte Developments for All-Solid-State Lithium Batteries: Classifications, Recent Advances and Synthesis Methods," J. Mater. Chem. A 12 (2024): 2250–2274.

[4] H. Pourzolfaghar, P.-Y. Wang, X.-Y. Jiang, et al., "Emerging trends and innovations in all-solid-state lithium batteries: A comprehensive review," Chem. Eng. J. 500 (2024): 157394.

[5] J. Zhang, L. Zhao, M. Chen, et al., "The challenges for the application of sulfide based all-solid-state lithium batteries," Renew. Sustain. Energy Rev. 207 (2025): 114829.

[6] Q. Wang, Y. Zhou, X. Wang, et al , "Designing lithium halide solid electrolytes," Nat. Commun. 15 (2024): 1050.

[7] Y. A. Mamus, V. M. K. R. Bhimaraju, D. H. Fabini, "Halide Superionic Conductors for All-Solid-State Batteries: Effects of Synthesis and Composition on Lithium-Ion Conductivity," ACS Energy Lett. 10 (2025): 710–719.

[8] F. Zhao, X. Chen, X. Chen, et al., "Promoting high-voltage stability through local lattice distortion of halide solid electrolytes," Nat. Commun. 14 (2023): 131.

[9] B. Hong, L. Gao, C. Li, et al., "All-solid-state batteries designed for operation under extreme cold conditions," Nat. Commun. 16 (2025): 143.

[10] N. B. Timusheva, A. A. Golubnichiy, A. V. Morozov, et al., "Chemical compatibility at the interface of garnet-type Ga-LLZO solid electrolyte and high-energy Li-rich layered oxide cathode for all-solid-state batteries," Sci. Rep. 15 (2025): 241.

[11] J. Sastre, X. Chen, A. Aribia, et al., "Fast Charge Transfer across the $Li_7La_3Zr_2O_{12}$ Solid Electrolyte/$LiCoO_2$ Cathode Interface Enabled by an Interphase-Engineered All-Thin-Film Architecture," ACS Appl. Mater. Interfaces. 12 (2020): 36196–36207.

[12] Z. Li, R. Yu, S. Weng, et al., "Tailoring Polymer Electrolyte Ionic Conductivity for Production of Low-Temperature Operating Quasi-All-Solid-State Lithium Metal Batteries," Nat. Commun. 14 (2023): 482.

[13] Y. Xiao, Y. Wang, S.-H. Bo, et al., "Understanding Interface Stability in Solid-State Batteries," Nat. Rev. Mater. 5 (2020): 105–126.

[14] S. Y. Lee, J. Rawal, J. Lee, et al., "Solid-State Electrolytes and Their Interfacial Properties: Implications for Solid-State Lithium Batteries," Electrochem. Energy Rev. 8 (2025): 9.

[15] Q. S. Zhao, C.-D. Wei, Y.-X. Hu, et al., "Insight into the Interface Chemical Stability of the Solid Electrolyte $Li_{1/2}La_{1/2}TiO_3$ and the Li/Li–In Alloy Anode," New J. Chem. 48 (2024): 15502–15512.

[16] Y. Deng, S. Jiao, T. Zhou, et al., "Understanding Lithium Loss in a Lithium Metal Anode with Liquid Electrolytes," MRS Energy Sustain. 12 (2025): 223–232.

[17] L. Ma, Y. Dong, N. Li, et al., "Current Challenges and Progress in Anode/Electrolyte Interfaces of All-Solid-State Lithium Batteries," eTransportation. 20 (2024): 100312.

[18] T. Asano, A. Sakai, S. Ouchi, et al., Solid halide electrolytes with high lithium-ion conductivity for application in 4 V class bulktype all-solid-state batteries, Adv. Mater. 30 (2018): e1803075.

[19] S.Wang,Q.Bai,A.M.Nolan, et al.,Lithium chlorides and bromides as promising solid-state chemistries for fast ion conductors with good electrochemical stability, Angew. Chem. Int. Ed. 58 (2019): 8039–8043.

[20] K. Kim, D. Park, H.-G. Jung, et al., Material design strategy for halide solid electrolytes Li_3MX_6(X = Cl,Br,and I)for all-solid state high-voltage Li-Ion batteries, Chem. Mater. 33 (2021): 3669–3677.

[21] J. Cheng, H. Zhang, Z. Wang, et al., "O_2−substituted Li-richened Li_2ZrCl_6 lattice towards superionic conductivity," J. Energy Storage 89 (2024): 111700.

[22] L. Zhou, C.Y. Kwok, A. Shyamsunder, et al., A new halospinel superionic conductor for high-voltage all solid state lithium batteries, Energy Environ. Sci. 13 (2020): 2056–2063.

[23] X. Li, J. Liang, J.T. Kim, et al., Highly stable halide-electrolyte-based all-solid-state Li–Se batteries, Adv. Mater. 34 (2022): 2200856.

[24] C. Yu, Y. Li, K.R. Adair, et al.,Tuning ionic conductivity and electrode compatibility of Li_3YBr_6 for high-performance all solid-state Li batteries, Nano Energy 77 (2020): 105097.

[25] X. Shi, Z. Zeng, H. Zhang, et al., Gram-scale synthesis of nanosized Li 3HoBr 6 solid electrolyte for all-solid-state Li-Se battery, Small Methods 5 (2021): 2101002.

[26] X. Shi, Z. Zeng, M. Sun, et al.,Fast Li-ion conductor of Li_3HoBr_6 for stable all-solid-state lithium–sulfur battery,Nano Lett. 21 (2021): 9325–9331.

[27] J. Liang, X. Li, S. Wang, et al., Site-occupation-tuned superionic Li_xScCl_{3+x} halide solid electrolytes for all-solid-state batteries, J. Am. Chem. Soc.142 (2020): 7012–7022.

[28] M. Lei, B. Li, H. Liu, et al., Dynamic Monkey Bar Mechanism of Superionic Li-ion Transport in $LiTaCl_6$, Angew. Chem. Int. Ed. 63 (2024): e202315628.

[29] K. Tuo, C. Sun, C. A. López, et al., New superionic halide solid electrolytes enabled by aliovalent substitution in $Li_{3-x}Y_{1-x}Hf_xCl_6$ for all-solid-state lithium metal based batteries, J. Mater. Chem. A 11 (2023): 15651-15662.

[30] K. Tuo, C. Sun, S. Liu, Recent Progress in and Perspectives on Emerging Halide Superionic Conductors for All-Solid-State Batteries, Electrochem. Energy Rev. 6 (2023): 17.

[31] G. M. Karpov, M. S. Mihaylov, T. B. Shatalova, et al., "The preparation and characterization of iron fluorides polymorphs FeF_3·0.33H2O and β-FeF_3·$3H_2O$ as cathode materials for lithium-ion batteries," J. Power Sources 449 (2020): 227557.

[32] Z. Liu, J. Liu, S. Xun, et al., "Low-cost iron trichloride cathode for all-solid-state lithium-ion batteries," Nat. Sustain. 7 (2024): 1492–1500.

[33] L. Zheng, W. Zheng, M. Xie, et al., "Interfacial Coupling with Halide Solid Electrolyte Enables High-Energy-Density and Reversible $FeCl_3$ Cathode for All-Solid-State Lithium Batteries," Adv. Energy Mater. 14 (2024): 2400088.

[34] R. Xiong, L. Yuan, R. Song, et al., "Solvent-Mediated Synthesis and Characterization of Li_3InCl_6 Electrolytes for All-Solid-State Li-Ion Battery Applications," ACS Appl. Mater. Interfaces. 16 (2024): 36281–36288.

[35] Y. Morino, N. Aoki, M. Nakamoto, "Revealing the Reductive Decomposition at the Interface of Li_3YCl_6–Lithium Metal," ACS Appl. Mater. Interfaces. 17 (2025):105-108.

[36] C. Zhang, H. Zhuang, Z. Qi, X. Liu, Y. Ren, "The effect of defects for the ion transport of Li_3ScCl_6 and Li_3InCl_6 with the interface of lithium metal anode: A first-principles study," Mater. Today Commun. 36 (2023): 105764.

[37] X. Li, J. Liang, X. Yang, et al., "Progress and Perspectives on Halide Lithium Conductors for All-Solid-State Lithium Batteries," Energy Environ. Sci. 13 (2020): 1429–1461.

[38] K. Tuo, F. Yin, C. Sun, "Low-Cost Halide Electrolytes $Li_{2+x}Hf_{1-x}Fe_xCl_6$ with Superior Ionic Conductivities for All-Solid-State Lithium–Metal Based Batteries," ACS Sustainable

Chem.Eng. 12 (2024): 6707–6717.

[39] C. Delmas, C. Fouassier, P. Hagenmuller, "Structural classification and properties of the layered oxides," Phys. B+C. 99 (1980): 81–85.

[40] N. H. Kwon, G. S. Park, J. H. Yun, Y. Kim, "The first-principles study on the thermal stability of $LiCoO_2$ cathode materials," J. Alloys Compd. 778 (2019): 405–410.

[41] L. D. Ellis, J. P. Allen, L. M. Thompson, "First-principles study on $LiCoO_2$ cathode materials," J. Electrochem. Soc. 164 (2017): A6054–A6059.

[42] P. Palvadeau, J. Venien, M. Spiesser, J. Rouxel, "Characterization of $LiFeCl_4$ and $AgFeCl_4$ ionic conductors," Solid State Ionics. 6 (1982): 231–236.

[43] G. Zhang, Z. Liu, Y. Ma, et al., "$Li_{2.9}Fe_{0.9}Zr_{0.1}Cl_6$ as Redox-Active Catholyte for Solid-State Li-Ion Batteries," Chem. Mater. 36 (2024): 10104–10112.

[44] S. Wang, Q. Bai, A. M. Nolan, et al., "Lithium Chlorides and Bromides as Promising Solid-State Chemistries for Fast Ion Conductors with Good Electrochemical Stability," Angew. Chem. Int. Ed. 58 (2019): 8039–8043.

[45] J. Liang, X. Li, S. Wang, et al., "Site-Occupation-Tuned Superionic Li_xScCl_{3+x} Halide Solid Electrolytes for All-Solid-State Batteries," J. Am. Chem. Soc. 142 (2020): 7012–7022.

[46] H. Kwak, D. Han, J. P. Son, et al., "Li^+ Conduction in Aliovalent-Substituted Monoclinic Li_2ZrCl_6 for All-Solid-State Batteries: $Li_{2+x}Zr_{1-x}M_xCl_6$ (M = In, Sc)," Chem. Eng. J. 437 (2022): 135413.

[47] H. Chen, S. Adams, "Bond Softness Sensitive Bond-valence Parameters for Crystal Structure Plausibility Tests," IUCr Journal. 4 (2017): 614–625.

[48] H. Chen, L. L. Wong, S. Adams, "SoftBV – a Software Tool for Screening the Materials Genome of Inorganic Fast Ion Conductors," Acta Crystallogr., B Struct. Sci., Cryst. Eng. Mater. 75 (2019): 18–33.

[49] Y. Duan, F. Hussain, H. Liu, et al., "Breaking the Conductivity-Capacity Trade-Off in MCl_6 Anionic Framework: Amorphous Oxyhalide Cathode Materials Enable $\approx$1100 Wh kg^{-1} at Cathode-Level in All-Solid-State Lithium Batteries," Adv. Mater. (2025): 2513544.

[50] S D. Xu, J. He, Y. He, et al., "Amorphization of halide solid electrolytes for lithium super-ionic conductivity," J. Mater. Chem. A 12 (2024) 27694–27702.

[51] H. Zhang, H. Liu, L.F.J. Piper, et al., "Oxygen Loss in Layered Oxide Cathodes for Li-Ion Batteries: Mechanisms, Effects, and Mitigation," Chem. Rev. 122 (2022) 5641–5681.

[52] R. Xu, Y. Wu, Z. Dong, et al., "Halide solid electrolytes in all-solid-state batteries: Ion transport kinetics, failure mechanisms and improvement strategies," Nano Energy 131 (2024) 110435.

[53] F. Sun, Z. Gao, Y. Yang, H. Chen, "Li−Fe−Cl Families as Novel Solid Electrolytes for All-Solid-State Batteries," ACS Appl. Mater. Interfaces. 16 (2024): 55666–55674.

[54] W. Hönle, A. Simon, "Darstellung und Kristallstrukturen von $LiGaBr_4$ und $LiGaBr_3$/Preparation and Crystal Structure of $LiGaBr_4$ and $LiGaBr_3$," Z. Naturforsch. B. 41 (1986): 1391–1398.

[55] K. Wang, Q. Ren, Z. Gu, et al., "A Cost-Effective and Humidity-Tolerant Chloride Solid Electrolyte for Lithium Batteries," Nat. Commun.12 (2021): 4410.

[56] W. Li, Z. Chen, Y. Chen, et al., "High-Voltage Superionic and Humidity-Tolerant $Li_{2.5}Sc_{0.5}Zr_{0.5}Cl_6$ Conductor for Lithium Batteries via Preferred Orientation," Chem. Eng. J. 455 (2023): 140509.

[57] X. Zhou, M. Jiang, Y. Duan, et al., "Multi-Electron Transfer Halide Cathode Materials Based on Intercalation-Conversion Reaction Towards All-Solid-State Lithium Batteries," Angew. Chem. Int. Ed. 64 (2025): e202416635.

[58] J. Fu, C. Wang, S. Wang, et al., "A cost-effective all-in-one halide material for all-solid-state batteries," Nature. 643 (2025): 111–118.

[59] Z. Liu, G. Zhang, J. Pepas, Y. Ma, H. Chen, "Li_2FeCl_4 as a Cost-Effective and Durable Cathode for Solid-State Li-Ion Batteries," ACS Energy Lett. 9 (2024): 5464–5470.

[60] D. Peng, R. Li, K. Xu, et al., "A Low-Strain Lithium Cathode Material $Li_{2-2x}Fe_{1+x}Cl_4$ for Halide-Based All-Solid-State Batteries," ACS Energy Lett. 10 (2025): 1421–1429.

[61] N. Tanibata, M. Kato, S. Takimoto, et al., "High Formability and Fast Lithium Diffusivity in Metastable Spinel Chloride for Rechargeable All-Solid-State Lithium-Ion Batteries," Adv. Energy Sustain. 1 (2020): 2000025.

[62] J. F. Baumgärtner, D. Isler, H. Q. Nguyen, et al., "A Highly Conductive Halospinel Cathode for All-Solid-State Batteries," ACS Energy Lett. 10 (2025): 5891–5899.

[63] C. Cao, M. R. Carbone, C. Komurcuoglu, et al., "Atomic insights into the oxidative

degradation mechanisms of sulfide solid electrolytes," Cell Rep. Phys. Sci. 5 (2024): 101909.

[64] J. G. Kim, H. R. Jung, M. H. Lee, et al., "High Ionic Conductivity Achieved in $Li_3Y(Br_3Cl_3)$ Mixed Halide Solid Electrolyte via Promoted Diffusion Pathways and Enhanced Grain Boundary," ACS Energy Lett. 5 (2020): 3313–3320.

[65] M. Jiang, T. Li, H. Long, et al., "Materials perspective on new lithium chlorides and bromides: insights into thermo-physical properties," Phys. Chem. Chem. Phys. 22 (2020): 22758–22767.

[66] M. Papakyriakou, F. Ahmed, J. Wang, et al., "Mechanical behavior of inorganic lithium-conducting solid electrolytes," J. Power Sources. 516 (2021): 230672.

[67] J. Liang, K. R. Adair, F. Zhao, et al., "Halide layer cathodes for compatible and fast-charged halides-based all-solid-state Li metal batteries," Angew. Chem. Int. Ed. 62 (2023): e202217081.

[68] K. Wang, Z. Gu, Z. Xi, et al., "Li_3TiCl_6 as ionic conductive and compressible positive electrode active material for all-solid-state lithium-based batteries," Nat. Commun. 14 (2023): 1396.

[69] X. Fan, E. Hu, X. Ji, et al., "High energy-density and reversibility of iron fluoride cathode enabled via an intercalation-extrusion reaction," Nat. Commun. 9 (2018): 2324.

[70] H. Liu, S. Liang, Y. Duan, et al., "Capacity-expanding O/Cl-bridged catholyte boosts energy density in zero-pressure all-solid-state lithium batteries," Natl. Sci. Rev. (2025): nwaf584.

[71] C. Liu, F. Roters, D. Raabe, "Role of grain-level chemo-mechanics in composite cathode degradation of solid-state lithium batteries," Nat. Commun. 15 (2024): 7970.

[72] Z. Zeng, J. Cheng, Y. Li, et al., "Composite cathode for all-solid-state lithium batteries: Progress and perspective," Mater. Today Phys. (2023): 101009.

[73] C. Jin, O. Sheng, G. Wei, et al., "Inhibiting and rejuvenating dead lithium in battery materials," Nat. Rev. Chem. 9 (2025): 553–568.

[74] Q. Liu, H. An, X. Wang, et al., "Effective transport network driven by tortuosity gradient enables high-electrochem-active solid-state batteries," Natl. Sci. Rev. 10 (2023): nwac272.

[75] D. Hlushkou, A. E. Reising, N. Kaiser, et al., "The influence of void space on ion transport in a composite cathode for all-solid-state batteries," J. Power Sources. 396 (2018): 246–256.

[76] C. Konig, V. Miss, L. Janin, et al., "Mitigating the Ion Transport Tortuosity in Composite Cathodes of All-Solid-State Batteries by Wet Milling of the Solid Electrolyte Particles," ACS Appl. Energy Mater. 6 (2023): 9356–9362.

[77] C. Yuan, W. Lu, J. Xu, "Electrochemical-mechanical coupling failure mechanism of composite cathode in all-solid-state batteries," Energy Storage Mater. (2023): 102834.

[78] D. Wang, X. Wu, Y. Ren, et al., "A review of interface optimization strategies for solid electrolytes and anode materials," Nanoscale Adv. 7 (2025) 4535–4550.

[79] S. Logesh, Y. W. Cheah, K. H. Ho, et al., "Flexural behaviours and heterogeneous interface fracture in overmoulded multi-material thermoplastic composites," Compos. Commun. (2024): 102152.

[80] X. Zhou, M. Jiang, Y. Duan, et al., "Multi-electron transfer halide cathode materials based on intercalation-conversion reaction towards all-solid-state lithium batteries," Angew. Chem. Int. Ed. 63 (2024): e202416635.

[81] N. Sun, Q. Liu, Y. Cao, et al., "Anisotropically electrochemical-mechanical evolution in solid-state batteries and interfacial tailored strategy," Angew. Chem. Int. Ed. 58 (2019): 13820–13826.

[82] Q. Li, H. Liu, Y. Ye, et al., "The critical importance of stack pressure in batteries," Nat Energy. 10 (2025): 1065–1075.

[83] A. Cronk, Y.-T. Chen, G. Deysher, et al., "Overcoming the interfacial challenges of $LiFePO_4$ in inorganic all-solid-state batteries," ACS Energy Lett. 8 (2023): 827–835.

[84] X. Wang, S. Huang, K. Guo, et al., "Directed and continuous interfacial channels for optimized ion transport in solid-state electrolytes," Adv. Funct. Mater. 32 (2022): 2206976.

[85] J. Yue, S. Zhang, X. Wang, et al., "Universal superionic conduction via solid dissociation of salts in van der Waals materials," Nat. Energy. 10 (2025): 1237–1250.

[86] N. W. Utomo, S. Hong, R. Sinha, et al., "Solid-state polymer-particle hybrid electrolytes: Structure and electrochemical properties," Sci. Adv. 10 (2024): eado4719.

[87] Z. Zhou, P. Lu, S. Liang, et al., "Embedding Fe-Based Redox Chemistry Into Low-Cost Oxyhalide Solid Electrolytes for High-Performance All-Solid-State Batteries," Adv. Mater. 4 (2026): 72694.

[88] L. Zhang, Y. Wang, A. Chu, et al., "Facet-selective growth of halide perovskite/2D semiconductor van der Waals heterostructures for improved optical gain and lasing," Nat. Commun. 15 (2024): 5484.

[89] W. Tang, F. Wang, S. Liang, et al., "Polyanion-stabilized amorphous halide electrolytes with low lithium content for all-solid-state lithium batteries," Nat. Commun. 4 (2026): 4863.

[90] P. Adeli, J. D. Bazak, K. H. Park, et al., "Boosting Solid-State Diffusivity and Conductivity in Lithium Superionic Argyrodites by Halide Substitution," Angew. Chem. Int. Ed. 58 (2019): 8681–8686.

[91] Y. K. Sun, S. T. Myung, B. C. Park, et al., "High-Energy Cathode Material for Long-Life and Safe Lithium Batteries," ACS. Nano. 8 (2014): 5738–5745.

[92] J. Heo, S.-K. Jung, I. Hwang, et al., "Amorphous iron fluorosulfate as a high-capacity cathode utilizing combined intercalation and conversion reactions with unexpectedly high reversibility," Nat. Energy. 8 (2023): 30–39.

[93] R. Li, D. Rao, J. Zhou, et al., "Amorphization-induced surface electronic states modulation of cobaltous oxide nanosheets for lithium-sulfur batteries," Nat. Commun. 12 (2021): 3102.

[94] X. Hua, A. S. Eggeman, E. Castillo-Martinez, et al., "Revisiting metal fluorides as lithium-ion battery cathodes," Nat. Mater. 20 (2021): 841–850.

[95] P. E. Lippens, M. E. Khalifi, M. Chamas, et al., "Mössbauer study of the electrochemical reaction with lithium of bimetallic Sn–M (M = Ti, V, Cr, Mn) alloys as negative electrodes for Li-ion batteries," Hyperfine Interact. 206 (2012): 35–46.

[96] X. Yang, X. Gao, S. Mukherjee, et al., "Designing principle for Ni-rich cathode materials with high cycling stability for next-generation lithium-ion batteries," Adv. Energy Mater. 10 (2020): 2001191.

[97] W. Fu, E. Zhao, Z. Sun, et al., Iron Fluoride–Carbon Nanocomposite Nanofibers as Free-Standing Cathodes for High-Energy Lithium Batteries, Adv. Funct. Mater. 28 (2018): 1801711.

[98] L. Wang, Z. Wu, J. Zou, et al., Li-free Cathode Materials for High Energy Density Lithium Batteries, Joule 3 (2019): 2086-2102.